

Principles of pattern selection for confined elastic shells

Ian Tobasco,^{1, 2, *} Yousra Timounay,^{3, 4} Desislava Todorova,⁵
Graham C. Leggat,³ Joseph D. Paulsen,^{3, 4, †} and Eleni Katifori^{5, ‡}

¹*Department of Mathematics, Statistics, and Computer Science,
University of Illinois at Chicago, Chicago, IL 60607, USA*

²*Department of Mathematics, University of Michigan, Ann Arbor, MI 48109, USA*

³*Department of Physics, Syracuse University, Syracuse, NY 13244, USA*

⁴*BioInspired Syracuse: Institute for Material and Living Systems, Syracuse University, Syracuse, NY 13244, USA*

⁵*Department of Physics and Astronomy, University of Pennsylvania, Philadelphia, PA 19104, USA*

Geometry-driven instabilities yield complex wrinkle patterns in thin elastic shells. Using experiments and simulations of shells confined to a liquid bath, we demonstrate the coexistence of ordered wrinkles and disordered regions whose layout is robust. This motivates the derivation of a coarse-grained “maximum coverage” problem predicting the patterns at large. The problem illuminates how a highly wrinkled shell behaves as an ideal locking material: its dual formulation defines the shell’s “locking stress”, a novel tensor for describing wrinkle patterns. General principles follow, including a classification of ordered wrinkles into three elementary types, and a Fermat-like principle for their topography in saddle-shaped shells. Such rules open avenues for the design and control of wrinkle patterns with applications from microfabrication to synthetic skins.

Geometry and mechanics underlie form, from the arches of antiquity to more recent, bio-inspired designs: in these, non-Euclidean geometry plays a leading role including, for instance, in the design of shape morphing membranes [1–3]. Geometry enters as well in the study of elastic patterns, involving wrinkles or some other fine-scale response [4–8]. Such patterns occur in diverse settings from textiles to graphene to biological films. A prototypical example appears in Fig. 1a,b, where square cutouts from curved shells wrinkle upon a water bath.

Here, we present a method for deducing the leading order features of wrinkle patterns driven by geometric incompatibilities and confining loads. Focusing on the example of a curved shell pressed flat, we show how the shell deforms and wrinkles to cover up a maximum area of the plane. We derive a general procedure solving this “maximum coverage” problem, in many cases reducing it to a simple geometric construction, e.g., inscribing or circumscribing a circle to the planform of the shell.

When tension pulls wrinkles taut, they organize to minimize the work done. This principle is known as tension field theory [9–11] and solving it — for instance, to determine the wrinkle direction *en masse* — is the first step in the far-from-threshold expansion that has explained many patterns [12–17]. Our experiments and simulations reveal, however, that organized patterns manifest with much weaker or even lacking tensile loads. And though wrinkles have been observed in situations of confinement, such as when a sheet is pressed between rigid spheres [18], it has remained up till now a significant challenge to predict the patterns that emerge.

Polystyrene films ($E = 3.4$ GPa, $\nu = 0.34$) of thickness $120 < t < 430$ nm were spin-coated on curved glass sub-

strates with radii of curvature $13 < R < 39$ mm. Cutouts of width $2.5 < W < 16$ mm were released to a flat air–water interface with surface tension $\gamma_{lv} = 0.072$ N/m and gravitational stiffness $K = \rho g$. The experiments reside in the limit of weak tension $\gamma_{lv}R^2 \ll YW^2$, moderately stiff substrate $KW^2 \gtrsim \gamma_{lv}$, and negligible bending stiffness $BKR^4 \ll Y^2W^4$ where $Y = Et$ and $B = Et^3/12(1 - \nu^2)$ are the stretching and bending moduli. Being shallow yet much larger than the characteristic substrate-dominated wrinkle wavelength $(B/K)^{1/4} \ll W \ll R$, the shells become approximately planar while forming intricate patterns as in Figs. 1a,b and 2. Ordered, wrinkled regions appear alongside disordered regions whose local features change between trials and under perturbation, whereas their layout remains. The patterns vary with the cut out shape and sign of the Gaussian curvature κ .

To explore the role of tension, we performed simulations of shells on flat liquid substrates using a finite-element method in ABAQUS, in the same general regime as the experiments albeit with $\gamma_{lv} = 0$. Notably, the simulations resulted in the same patterns as the experiments, with matching ordered regions and the layout of the disordered regions the same. Two representative simulations appear in Fig. 1a,b. Others with non-constant curvature reveal the patterns are, to leading order, independent of the precise value of $\kappa(x)$ and depend only on its sign (see Fig. S1 of the *Supplementary Information* (SI)). These and other remarkably robust features of geometry-driven wrinkling will be explained.

Wrinkle patterns can be deduced by minimizing an energy $U = U_{\text{elastic}} + U_{\text{substrate}} = (U_{\text{stretch}} + U_{\text{bend}}) + (U_{\text{grav}} + U_{\text{surf}})$. The central unknown is the “effective” or leading order displacement of the cut out shell, initially the graph of a function $p(x)$ over its planform Ω . As in [15, 16, 19], we posit the existence of an “asymptotically isometric” regime wherein minimizers have negligible albeit non-zero stretching. Its existence is not *a priori* clear as minimizers are generally unknown, but can nevertheless

* itobasco@uic.edu

† jdpulse@syr.edu

‡ katifori@sas.upenn.edu

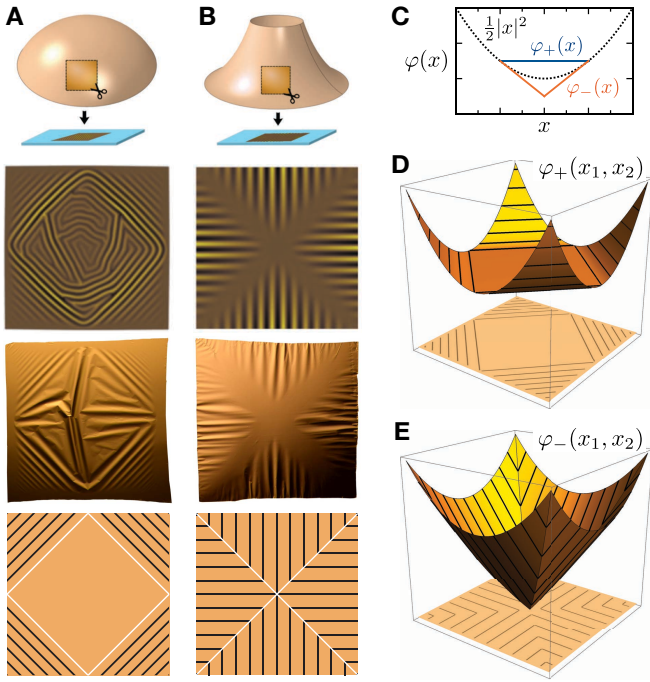


FIG. 1. Confined shells wrinkle along stable lines. Patterns result when square cutouts of spherical (A) and saddle-shaped (B) shells are forced flat. Simulations and experiments with vanishing or weak tensile loads show robust regions of ordered wrinkles coexisting in some cases with disordered regions, the local features of which are statistical as in (A). The patterns are predicted by the method of stable lines, derived herein. Stable lines indicate ordered wrinkle peaks and troughs. They arise upon projection of an optimal convex extension $\varphi(x)$ of the function $\frac{1}{2}|x|^2$ to the planform of the shell (C-E). For sphere/saddle-shaped shells the largest/smallest convex extension $\varphi_+(x)$ or $\varphi_-(x)$ applies.

less be deduced from suitable hypotheses as explained in the SI following [20]. There, we show that the shell is effectively planar with energy $U \approx \gamma_{\text{eff}}\Delta A$ to leading order in $\gamma_{\text{eff}} = 2\sqrt{BK} + \gamma_{lv} \rightarrow 0$. The effective in-plane displacement $u_{\text{eff}}(x)$ minimizes the areal change

$$\Delta A = \int_{\Omega} \frac{1}{2} |\nabla p|^2 dx - \int_{\partial\Omega} u_{\text{eff}} \cdot \hat{\nu} ds \quad (1)$$

while its strain $\varepsilon_{\text{eff}}(x) = e(u_{\text{eff}}) - \frac{1}{2}\nabla p \otimes \nabla p$ remains tension-free (≤ 0). We recognize $\Delta A = A_{\text{initial}} - A_{\text{proj}}$ as a measure of the area “lost” to infinitesimal wrinkling; minimizing it maximizes coverage of the plane. Similar area-based models have illuminated situations with weak but dominant surface tension [21–24]. Here, γ_{eff} emerges as an effective surface tension promoting the shell to maximize coverage even when $\gamma_{lv} = 0$. We note a connection with the “bending-induced” tension identified in [19] using the proposed Gauss-Euler elastica principle, wherein the condition of asymptotic isometry enters as a constraint. Our derivation of the maximum coverage problem — $\min \Delta A$ subject to $\varepsilon_{\text{eff}} \leq 0$ — justifies and

simplifies the G-E elastica to leading order.

While wrinkle patterns can be determined by maximizing coverage directly, the dual formulation is not only easier to solve but also reveals a novel tensor for describing wrinkle patterns called the “locking stress”. Our idea is to treat the highly wrinkled shell as a so-called ideal locking material [25], which exhibits tension-free strain $\varepsilon_{\text{eff}} \leq 0$ with negligible stress below a threshold where a component vanishes and wrinkles “lock” into place. Other examples include certain biological tissues that deform freely up to a threshold strain [26]. Confined shells behave similarly as wrinkles put under compression readily reorganize, a fact reflected by the metastable behavior of the disordered part.

We now derive the locking stress $\sigma_L(x)$ of a highly wrinkled, effectively planar shell. First, it is a divergence-free symmetric tensor that is compression-free (≥ 0). Second, it is perpendicular to the effective strain $\varepsilon_{\text{eff}}(x)$. Third, its boundary values are determined implicitly through the solution of a locking stress problem dual to the maximum coverage one and derived in its most general form in the SI. For simply connected shells (lacking holes), an Airy potential $\varphi(x)$ for the locking stress $\sigma_L = \nabla^\perp \nabla^\perp \varphi$ is readily introduced yielding

$$\min \Delta A = \max \int_{\Omega} \left(\varphi - \frac{1}{2}|x|^2 \right) \kappa dx \quad (2)$$

amongst all convex $\varphi(x)$ equaling $\frac{1}{2}|x|^2$ outside the planform Ω (Fig. 1c-e). Note σ_L is not the usual stress of the shell; for one, its normal boundary component need not equal γ_{lv} . Instead, it arises as a Lagrange multiplier for the tension-free constraint predicting the wrinkle direction in the ordered part where it is non-zero. There, “stable lines” passing by definition through the principal direction of positive σ_L run asymptotically parallel to wrinkle peaks and troughs. Disorder restricts to where $\sigma_L = 0$ as there stable lines do not exist.

This powerful method of stable lines for predicting wrinkle patterns is demonstrated in Figs. 1 and 2. We note the existence of explicit solution formulae and accompanying geometric constructions when the (possibly non-constant) Gaussian curvature is of a known sign. If $\kappa(x) > 0$, the locking stress is that of the largest convex extension $\varphi_+(x) = \min \sum_i \theta_i \frac{1}{2}|y_i|^2$ over pairs and triples $\{y_i\} \subset \partial\Omega$ with barycenter $x = \sum_i \theta_i y_i$. The formula describes an optimal partition of the shell into ordered and convex disordered parts, where stable lines connect boundary points and do not meet in the bulk. If $\kappa(x) < 0$, the locking stress is given by the smallest convex extension $\varphi_-(x) = \frac{1}{2}|x|^2 - \min \frac{1}{2}|x - y|^2$ over $y \in \partial\Omega$. Stable lines extend perpendicularly from the boundary to the medial axis and disorder is ruled out.

Once the shell’s locking stress $\sigma_L(x)$ is known, its effective strain $\varepsilon_{\text{eff}}(x)$ and out-of-plane displacement $w(x)$ can be recovered via its “defect measure” $\mu(dx) = \langle \nabla w \otimes \nabla w \rangle$ which obeys $\varepsilon_{\text{eff}} + \frac{1}{2}\mu = 0$. Angle brackets denote an asymptotic averaging defined in the SI for patterns from diffuse wrinkles to concentrated folds [27]. The following

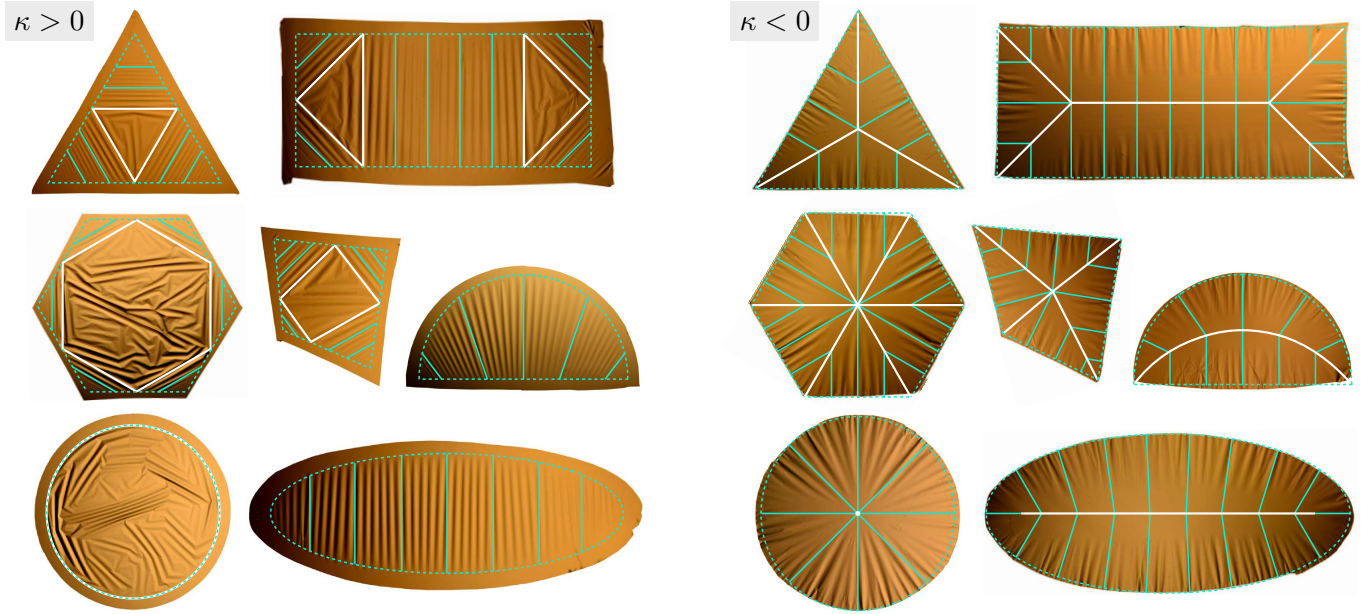


FIG. 2. **Floating shells and their stable lines.** Stable lines (blue) predict ordered wrinkle peaks and troughs. Geometric constructions produce explicit formulae, even absent obvious symmetries. When the shell is saddle-shaped ($\kappa < 0$), the lines obey a Fermat-like principle following paths of quickest approach to the edge. Disorder is ruled out and wrinkles decay towards the medial axis (white). Spherical shells ($\kappa > 0$) are less explicit but just as easily solved: stable lines connect boundary points in an optimal partition of the shell into ordered and convex disordered parts (white). Their layout is often revealed by inscribing or fitting a maximal circle into the planform, though sometimes a circumscribed circle applies. Wrinkles decay towards a small tensional rim. Dotted lines indicate ideal planforms used in the predictions. Experimental parameters are in Tables S1 and S2.

boundary value problem is solved: first, Gauss's *Theorema Egregium* holds in the form $\partial_{12}\mu_{12} - (\partial_{11}\mu_{22} + \partial_{22}\mu_{11})/2 = \kappa$ expressing conservation of curvature for asymptotic isometries; second, $\sigma_L : \mu = 0$ due to the perpendicularity of locking stress and effective strain; third, $(\sigma_L)_{\hat{\tau}\hat{\tau}}\mu_{\hat{\tau}\hat{\tau}} = 0$ at $\partial\Omega$ reflecting a possible concentration of the tangential component of the locking stress. Integration yields the amplitude to first approximation in the ordered part as in Fig. 3, with corrections arising for a non-constant wrinkle direction, e.g., bend or splay [28]. Various properties follow, such as the fact that ordered wrinkles can only meet where $\kappa(x) < 0$. This is consistent with the organizing role played by the medial axis in negatively curved shells; it also predicts the generic appearance of disorder in arbitrarily curved shells.

We close with a far-reaching classification of wrinkle patterns implied by the method of stable lines. Since the locking stress $\sigma_L(x) \sim \hat{T} \otimes \hat{T}(x)$ wherever stable lines parallel to $\hat{T}(x)$ exist, an Airy potential $\varphi(x)$ describes a developable surface, i.e., one with zero Gaussian curvature. Away from singularities, the non-planar part of any developable surface consists of cylinders, cones, or so-called tangential developables [29]. Upon projection, we discover the three classes of ordered wrinkle patterns: “cylindrical” patterns with parallel stable lines, “conical” patterns with radial lines, and “tangential” patterns with lines meeting along a curve. Each class appears in Fig. 2. The principles of pattern selection described here open

a promising direction towards their design and control. Patterns produced by buckling rather than by direct intervention can be made easily and rapidly at large. Furthermore, the results are not necessarily permanent and

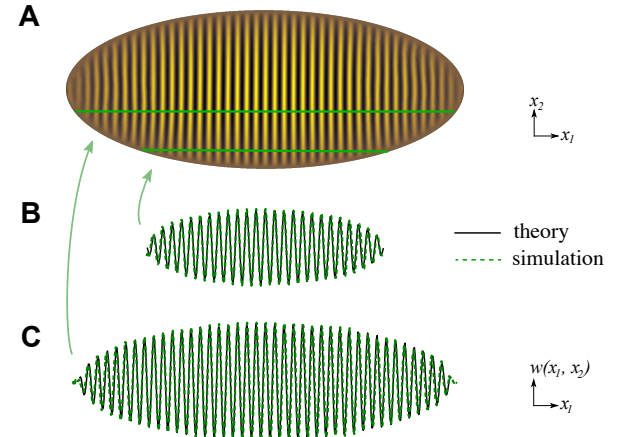


FIG. 3. **Amplitude of a positively curved ellipse.** The wrinkle amplitude (black) is recovered by integrating Gauss's *Theorema Egregium* along stable lines and requiring that it vanish at the boundary in this case, yielding excellent agreement with the simulated displacement (green). Only the wrinkle wavelength and a global phase shift are fixed.

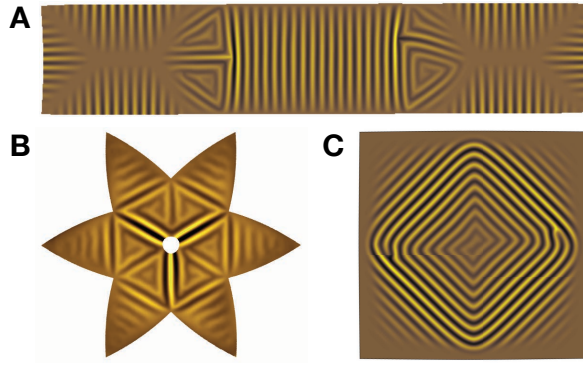


FIG. 4. **Open questions.** Stable lines are in principle capable of capturing the behavior of (A) shells having curvature of both signs ($\kappa > 0$ in the middle) and (B) shells with holes, though explicit formulae are so far lacking in these cases. (C) Another question regards the presence of order within generically disordered regions absent stable lines (cf. Fig 1a). Empirically, this depends on the finite wrinkle wavelength.

can be reconfigured by tuning bulk geometric or mechanical properties. Such features are attractive for a wide range of applications including anti-fouling coatings, lens

arrays, smart windows, and tunable adhesives [30–32].

Open challenges include developing efficient methods for finding the stable lines of general shells, including ones with Gaussian curvature of variable sign or with holes as in Fig. 4a,b. Others regard sensitivity to shape: perturbations as small as a few wrinkles can have long-range effects, even changing disorder to order sometimes (see Fig. S3). Finally, though regions lacking stable lines are currently understood as generically disordered, sometimes order presents as in Fig. 4c (see also Fig. S4). Often, this occurs when the region contains relatively few wrinkles. Progress on these issues, when combined with the methodology uncovered here, will provide a toolkit for bridging the gap between low-resolution, large-scale properties and fine-scale elastic patterns.

Acknowledgements — We thank B. Davidovitch, V. Démery, C. R. Doering, G. Francfort, R. V. Kohn, and N. Menon for helpful discussions. This work was supported by NSF awds. DMS-1812831 and DMS-2025000, a U. Mich. Van Loo Postdoc. Fellowship (IT); NSF awd. DMR-CAREER-1654102 (YT, JDP); NSF awd. PHY-CAREER-1554887, U. Penn. MRSEC awd. DMR-1720530 and CEMB awd. CMMI-1548571, and a Simons Foundation awd. 568888 (EK).

[1] A. S. Gladman, E. A. Matsumoto, R. G. Nuzzo, L. Mahadevan, and J. A. Lewis, *Nat. Mater.* **15**, 413 (2016).

[2] H. Aharoni, Y. Xia, X. Zhang, R. D. Kamien, and S. Yang, *Proc. Natl. Acad. Sci.* **115**, 7206 (2018).

[3] E. Siéfert, E. Reyssat, J. Bico, and B. Roman, *Nat. Mater.* **18**, 24 (2019).

[4] B. Li, Y.-P. Cao, X.-Q. Feng, and H. Gao, *Soft Matter* **8**, 5728 (2012).

[5] N. Stoop, R. Lagrange, D. Terwagne, P. M. Reis, and J. Dunkel, *Nat. Mater.* **14**, 337 (2015).

[6] H. Aharoni, D. V. Todorova, O. Albarrán, L. Goehring, R. D. Kamien, and E. Katifori, *Nat. Commun.* **8**, 15809 (2017).

[7] J. D. Paulsen, *Annu. Rev. Condens. Matter Phys.* **10**, 431 (2019).

[8] D. Vella, *Nat. Rev. Phys.* **1**, 425 (2019).

[9] H. Wagner, Z. Flugtech. Motorluftshifffahrt **20**, 200 (1929).

[10] A. C. Pipkin, *IMA J. Appl. Math.* **36**, 85 (1986).

[11] D. J. Steigmann, *Proc. Roy. Soc. London Ser. A* **429**, 141 (1990).

[12] B. Davidovitch, R. D. Schroll, D. Vella, M. Adda-Bedia, and E. A. Cerdá, *Proc. Natl. Acad. Sci.* **108**, 18227 (2011).

[13] H. King, R. D. Schroll, B. Davidovitch, and N. Menon, *Proc. Natl. Acad. Sci.* **109**, 9716 (2012).

[14] P. Bella and R. V. Kohn, *Comm. Pure Appl. Math.* **67**, 693 (2014).

[15] E. Hohlfeld and B. Davidovitch, *Phys. Rev. E* **91**, 012407 (2015).

[16] D. Vella, J. Huang, N. Menon, T. P. Russell, and B. Davidovitch, *Phys. Rev. Lett.* **114**, 014301 (2015).

[17] M. Taffetani and D. Vella, *Philos. Trans. Roy. Soc. A* **375**, 20160330 (2017).

[18] J. Hure, B. Roman, and J. Bico, *Phys. Rev. Lett.* **109**, 054302 (2012).

[19] B. Davidovitch, Y. Sun, and G. M. Grason, *Proc. Natl. Acad. Sci.* **116**, 1483 (2019).

[20] I. Tobasco, [arXiv:1906.02153](https://arxiv.org/abs/1906.02153).

[21] Z. Yao, M. Bowick, X. Ma, and R. Sknepnek, *EPL* **101**, 44007 (2013).

[22] J. D. Paulsen, V. Démery, C. D. Santangelo, T. P. Russell, B. Davidovitch, and N. Menon, *Nat. Mater.* **14**, 1206 (2015).

[23] J. D. Paulsen, V. Démery, K. B. Toga, Z. Qiu, T. P. Russell, B. Davidovitch, and N. Menon, *Phys. Rev. Lett.* **118**, 048004 (2017).

[24] M. Ripp, V. Démery, T. Zhang, and J. Paulsen, *Soft Matter* (2020), 10.1039/D0SM00250J.

[25] W. Prager, *Trans. Soc. Rheol.* **1**, 169 (1957).

[26] W. Prager, *Q. Appl. Math.* **27**, 128 (1969).

[27] L. Pocivavsek, R. Dellsy, A. Kern, S. Johnson, B. Lin, K. Y. C. Lee, and E. Cerdá, *Science* **320**, 912 (2008).

[28] O. Tovkach, J. Chen, M. M. Ripp, T. Zhang, J. D. Paulsen, and B. Davidovitch, *Proc. Natl. Acad. Sci.* **117**, 3938 (2020).

[29] D. J. Struik, *Lectures on classical differential geometry* (Dover Publications, Inc., New York, 1988).

[30] L. Pocivavsek, J. Pugar, R. O'Dea, S.-H. Ye, W. Wagner, E. Tzeng, S. Velankar, and E. Cerdá, *Nat. Phys.* **14**, 948 (2018).

[31] S. Yang, K. Khare, and P.-C. Lin, *Adv. Funct. Mater.* **20**, 2550 (2010).

[32] P. M. Reis, *J. Appl. Mech.* **82**, 111001 (2015).

Supplementary Information for: “Principles of pattern selection for confined elastic shells”

Tobasco et al.

CONTENTS

- I. Supplementary Tables
- II. Supplementary Figures
- III. Supplementary Text
 - A. Elastic energy minimization and the emergence of maximum coverage
 - 1. Energies and non-dimensional groups
 - 2. Asymptotic isometries in and out of equilibrium
 - 3. Derivation of the maximum coverage problem
 - B. Highly wrinkled shells as ideal locking materials
 - 1. The locking stress
 - 2. Orthogonality of stress and strain
 - 3. The method of stable lines
 - C. Solution of the locking stress problem for simply connected shells
 - 1. The relaxed Airy potential formulation
 - 2. Solutions and geometric constructions, positive curvature
 - 3. Solutions and geometric constructions, negative curvature
 - D. Recovering the effective strain and r.m.s. amplitude
 - 1. Defect measures and asymptotic isometries
 - 2. A boundary value problem for defect measures
 - 3. On the sign of curvature where ordered wrinkles meet
 - E. Worked example: a positively curved ellipse
 - F. Future directions
 - 1. Sensitivity to perturbations of shape
 - 2. Order in generically disordered regions
- IV. Materials and Methods
 - A. Film preparation
 - B. Finite element simulations
 - C. Parameter ranges
 - 1. Experimental ranges
 - 2. Simulation ranges
- References

I. SUPPLEMENTARY TABLES

S1

	Planform shape	R [mm]	t [nm]	W [mm]	
S2	Fig. 1a	Square	25.7	167	6.7
S4	Fig. 2	Triangle	34.5	152	6.5
S4		Rectangle	38.6	162	9.5
S4		Hexagon	25.7	158	8.4
S4		Tangential polygon	25.7	166	5.3
S4		Semicircle	34.5	151	7.7
S5		Circle	34.5	157	7.7
S5		Ellipse	25.7	152	8.6

S6

TABLE S1. Experimental parameters for the spherical shell cutouts ($\kappa > 0$) shown in the main text. Radius of curvature R , thickness t , and planform width W are reported. The choice of representative width depends on the shape, and is taken to be a radius, semi-major axis length, or half of a long diagonal or side as appropriate.

S11

	Planform shape	$ R_i $ [mm]	t [nm]	W [mm]	
S11	Fig. 1b	Square	25, 34	408	5.1
S12	Fig. 2	Triangle	25, 34	331	4.5
S13		Rectangle	25, 34	242	5.0
S13		Hexagon	25, 34	334	5.0
S13		Tangential polygon	25, 34	378	5.9
S14		Semicircle	25, 34	389	6.3
S14		Circle	25, 34	427	6.3
S14		Ellipse	25, 34	325	8.2

S14

TABLE S2. Experimental parameters for the saddle-shaped shell cutouts ($\kappa < 0$) shown in the main text. Unsigned principal radii of curvature $|R_1|$ and $|R_2|$, thickness t , and planform width W are reported.

S17

	Planform shape	R [cm]	t [μ m]	W [cm]	K [Pa/m]	
S18	Fig. 1a	Square ($\kappa > 0$)	20	5	3.05	2000
S18	Fig. 1b	Square ($\kappa < 0$)	6.4, 7.8	1	1	100
S18	Fig. 3	Ellipse ($\kappa > 0$)	20	2	5	100

S18

S18

S18

S18

S18

S18

S19

TABLE S3. Parameters for the simulated shells shown in the main text. Radius of curvature R (unsigned principal radii for $\kappa < 0$), thickness t , planform width W , and substrate stiffness K are reported. A Young's modulus of $E = 2$ MPa and Poisson's ratio of $\nu = 0.495$ is used.

II. SUPPLEMENTARY FIGURES

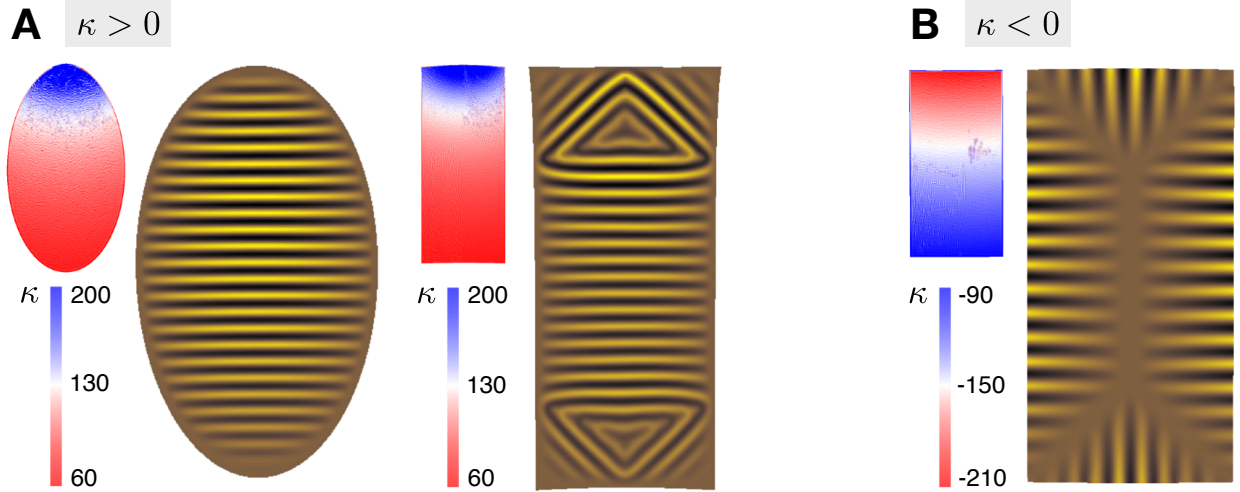


FIG. S1. **Shells having non-constant Gaussian curvature of a definite sign.** Colormaps of the initial Gaussian curvature $\kappa(x)$ of three shells (top view) and their effectively planar, wrinkled states in the (a) positively curved and (b) negatively curved cases, from the simulations. The gross features of the patterns are independent of the precise values of the curvature but depend strongly on its overall sign. This is as predicted by the method of stable lines. Parameters: (a) $t = 7 \mu\text{m}$, $W = 4 \text{ cm}$ for the ellipse and 3.6 cm for the rectangle, $K = 2000 \text{ Pa/m}$; (b) $t = 2 \mu\text{m}$, $W = 2 \text{ cm}$, $K = 100 \text{ Pa/m}$. Gaussian curvature κ is in units of cm^{-2} . In both, $E = 2 \text{ MPa}$ and $\nu = 0.495$.

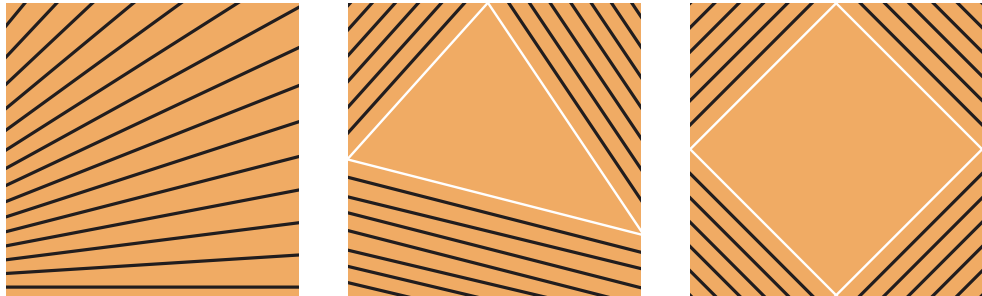


FIG. S2. **Stable lines follow optimal partitions of positively-curved shells.** Each diagram represents an admissible partition of a positively-curved square into ordered, wrinkle regions covered by candidate stable lines (black) and leftover, possibly disordered regions (bordered in white). Stable lines extend to the boundary and leftover regions are convex. Optimization over all such partitions produces the predicted one on the right. This corresponds to finding the largest convex extension $\varphi_+(x)$ of $\frac{1}{2}|x|^2$ into the square.

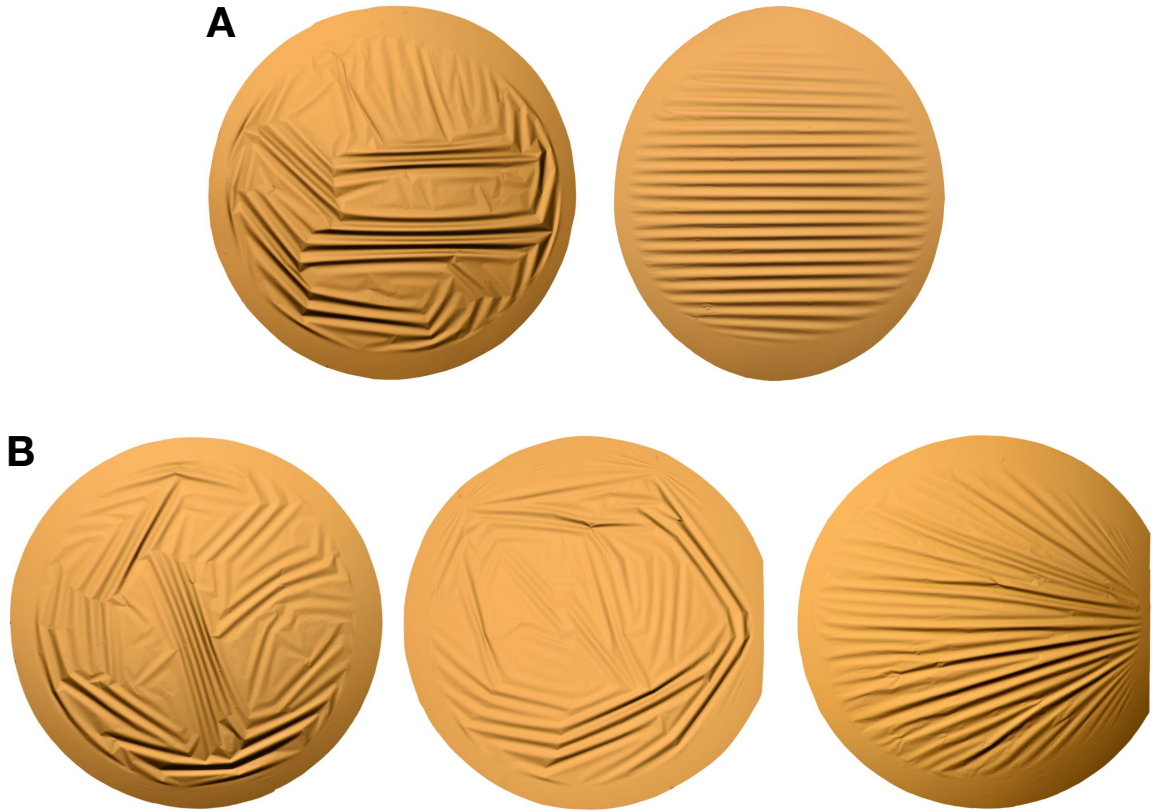


FIG. S3. **Sensitivity to perturbations of shape.** (a) Spherical shells with elliptical planforms, with larger ellipticity on the right. The left planform has aspect ratio 1.02 and presents a disordered response. The method of stable lines predicts parallel wrinkles as on the right for any ellipticity. (b) Spherical shells with circular planforms and a small slice removed. The size of the cut increases from left to right, with no cut for the leftmost shell. The response becomes ordered with a sufficiently large cut, whereas stable lines describe the same radial pattern for any cut. Determining the physical balance that sets the threshold for these transitions is an open challenge. Parameters: (a) $R = 25.7$ mm, $W = 7.7$ mm, $143 < t < 160$ nm; (b) $R = 34.5$ mm, $W = 7.8$ mm, $151 < t < 157$ nm.

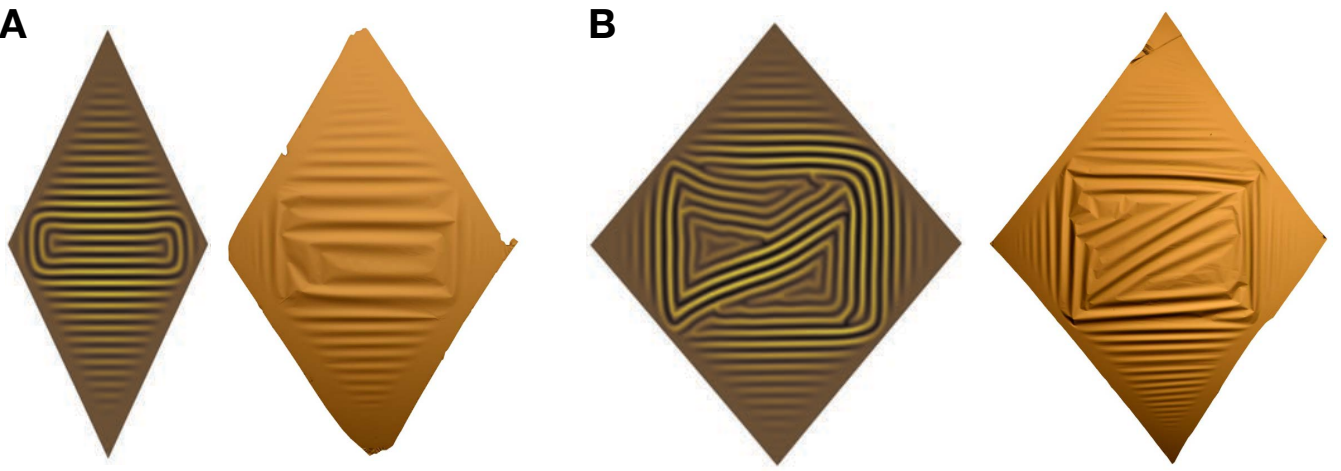


FIG. S4. **Order in disordered regions.** (a) Ordered patterns in the generically disordered central region of a spherical rhombus. (b) Central region displaying disorder consistent with the predicted absence of stable lines (by the inscribed circle construction). Empirically, order occurs when the wrinkle wavelength is comparable to the region's width. Constructing a fundamental description of this is an open challenge. In both panels, the left image is from simulation and the right image is from experiment. Parameters: $R = 25.7$ mm and $t = 167$ nm in the experiments, with $W = 5.8$ mm in (a) and $W = 9.4$ mm in (b); $R = 10$ cm and $t = 5 \mu\text{m}$ in the simulations, with $W = 4.3$ cm in both. The simulations use a shell having $E = 2$ MPa and $\nu = 0.495$, and a substrate with $K = 2000$ Pa/m. The representative width is one half of the long diagonal.

III. SUPPLEMENTARY TEXT

Here we describe the steps leading from the principle of minimum energy to the coarse-grained prediction of wrinkle patterns by the method of stable lines. Though our argument builds off of the approach of the first author in [1], the current presentation is aimed at a broad audience and can be read essentially independently of the reference. For the reader interested in detailed mathematical proofs we have included various pointers locating the relevant details.

We begin in Section III A by showing how the maximum coverage problem introduced in the main text derives from coarse-graining the energy of a confined elastic shell. This prompts us to treat the shell as an ideal locking material, which we do for general planforms defining the concepts of “locking stress” and “stable lines” in Section III B, and for simply connected planforms using Airy potentials in Section III C. Once the locking stress and stable lines of a shell are known, its effective strain and displacements can be recovered as in Section III D. The reader looking for an example to help anchor the theory should consult Section III E. There, we apply it to the case of a positively curved ellipse recovering the theoretical prediction in Figure 3 of the main text. We close with a brief discussion of future directions in Section III F, focusing on the intriguing questions of sensitivity to shape and “incidental” order.

A. Elastic energy minimization and the emergence of maximum coverage

We consider the deformation of a naturally curved, thin elastic shell pressed flat by

- (i) fully wetted adhesion to a planar liquid bath, or
- (ii) attachment to a planar Winkler foundation, i.e., a bed of linear springs.

Our purpose in treating these apparently different setups is make the point that, regardless of the presence or lack of a weak tensile restoring force, elastic patterns arising from geometric incompatibility and confinement are unified through a common maximum coverage problem dictating their features at leading order.

Section III A 1 presents the basic energies to be minimized and identifies the parameter regime of interest. Section III A 2 recalls the concept of “asymptotic isometries” which serves to motivate the coarse-graining we do. Finally, in Section III A 3 we derive the maximum coverage problem by passing to the effectively planar limit. Along the way it will become clear the precise sense in which we coarse-grain.

1. Energies and non-dimensional groups

We suppose the shell is initially the graph of a function $p(x)$ over its reference planform $\Omega \subset \mathbb{R}^2$ with Euclidean coordinates $x = (x_1, x_2)$. Its deformation

$$(x, p(x)) \mapsto (x_1 + u_1(x), x_2 + u_2(x), w(x))$$

is specified by its in- and out-of-plane displacements $u(x) = (u_1, u_2)$ and $w(x)$ parallel and perpendicular to the initial substrate. Provided the shell is shallow, its deformation can be found by minimizing the energy [2–4]

$$\begin{aligned} U &= U_{\text{elastic}} + U_{\text{substrate}} = (U_{\text{stretch}} + U_{\text{bend}}) + (U_{\text{sub}} + U_{\text{surf}}), \quad \text{with} \\ U_{\text{stretch}} &= \frac{1}{2} \int_{\Omega} \sigma : \varepsilon \, dx, \quad U_{\text{bend}} = \frac{B}{2} \int_{\Omega} \left[|\Delta(w - p)|^2 - 2(1 - \nu) \det \nabla \nabla(w - p) \right] \, dx, \\ U_{\text{sub}} &= \frac{K}{2} \int_{\Omega} |w|^2 \, dx, \quad U_{\text{surf}} = \gamma_{\text{lv}} \left(\int_{\Omega} \frac{1}{2} |\nabla p|^2 \, dx - \int_{\partial\Omega} u \cdot \hat{v} \, ds \right), \quad \text{and} \\ \sigma_{11} &= \frac{Y}{1 - \nu^2} (\varepsilon_{11} + \nu \varepsilon_{22}), \quad \sigma_{22} = \frac{Y}{1 - \nu^2} (\varepsilon_{22} + \nu \varepsilon_{11}), \quad \sigma_{12} = \frac{Y}{1 - \nu^2} (\varepsilon_{12} - \nu \varepsilon_{12}). \end{aligned}$$

Here, $A : B = \sum_{ij} A_{ij} B_{ij}$ is the usual tensor inner product and $|\cdot|$ is the Euclidean norm. The outwards pointing unit normal and arclength element at $\partial\Omega$ are \hat{v} and ds . Physical parameters include the stretching and bending moduli $Y = Et$ and $B = Et^3/12(1 - \nu^2)$ of the shell, with E its Young’s modulus, ν its Poisson’s ratio, and t its thickness. We use an isotropic Hooke’s law relating the stress σ to the strain ε . Let W be a representative width

for the planform, e.g., the radius of a disc or semi-major axis length of an ellipse, and let R be a representative radius of curvature for the shell so that its (generally non-constant) Gaussian curvature $\kappa(x) = (R_1 R_2)^{-1} \sim R^{-2}$ where R_1, R_2 are its initial principal radii. The substrate stiffness is K and the liquid–vapor surface tension is γ_{lv} . For the Winkler foundation $\gamma_{\text{lv}} = 0$; for the bath $K = \rho g$ where ρ is its density and g its gravitational acceleration.

Shallowness of the shell entails that its bare, geometry-induced strain arising in direct attachment to the plane is much less than one, i.e., $W^2/R^2 \ll 1$. This permits various simplifications, including the use of the von Karman-like formula for the strain

$$\varepsilon(x) = e(u) + \frac{1}{2} \nabla w \otimes \nabla w - \frac{1}{2} M \quad (\text{S1})$$

with geometric “misfit” $M(x) = \nabla p \otimes \nabla p$, as well as the approximation of the Gaussian curvature

$$\kappa(x) \approx \det \nabla \nabla p = -\frac{1}{2} \operatorname{curlcurl} M$$

which we understand as an equality henceforth. We write $e_{ij}(u) = (\partial_i u_j + \partial_j u_i)/2$ with $i, j \in \{1, 2\}$ for the linear strain of u and $(X \otimes X)_{ij} = X_i X_j$ for the dyadic product. The operator $\operatorname{curlcurl} M = \partial_{11} M_{22} + \partial_{22} M_{11} - 2\partial_{12} M_{12}$, a combination we recall from the appearance of Gauss’ *Theorema Egregium* in the main text. The reference area element dx approximates the true area element dA of the shell; other such simplifications are implicit above. We note that while the addition of $\gamma_{\text{lv}} \int_{\Omega} \frac{1}{2} |\nabla p|^2$ does not alter equilibria, it will serve to simplify the form of the expansion $U \approx \gamma_{\text{eff}} \Delta A$ to be derived.

Finally, we point out that our analysis is not limited to the specific setup of a shallow shell pressed flat, but applies *mutatis mutandis* to a shell on a curved substrate with small misfit or, more generally, to a situation where the misfit does not derive from an imposed change of shape but is instead due, e.g., to differential swelling or growth [5]. In these setups, the curvature of the shell $\kappa(x)$ must be replaced by the difference between the intrinsic and imposed curvatures $\Delta\kappa(x) = \kappa_{\text{intrinsic}} - \kappa_{\text{imposed}}$. With this, we can easily compare our results with those in the surrounding literature which, for instance, treat the case of a naturally flat plate pressed onto a sphere or a saddle-shape giving $\Delta\kappa < 0$ or > 0 .

Coming back to the problem at hand, we consider minimizing U in the following regime: we suppose the surface tension is either absent with $\gamma_{\text{lv}} = 0$ or else is not much larger than the substrate forces in that $\gamma_{\text{lv}} \lesssim KW^2$; we suppose the effective tension $\gamma_{\text{eff}} := 2\sqrt{BK} + \gamma_{\text{lv}}$ is much smaller than the bare, geometry-induced stress $\sigma_{\text{geom}} := YW^2/R^2$; finally, we suppose the substrate-dominated wrinkle wavelength $\lambda_{\text{sub}} := 2\pi(B/K)^{1/4}$ is much smaller than the planform width W . The latter conditions allow for the shell to become highly wrinkled, while the former ensures any applied tension is sufficiently weak. Introducing the non-dimensional groups

$$b := \frac{B}{YW^2} \cdot \frac{R^2}{W^2} = \text{bendability}^{-1}, \quad k := \frac{KR^2}{Y} = \text{deformability}^{-1}, \quad \gamma := \frac{\gamma_{\text{lv}}}{Y} \cdot \frac{R^2}{W^2} = \text{confinement}^{-1} \quad (\text{S2})$$

familiar from other studies of elastocapillarity (see, e.g., [6, 7]) this regime becomes

$$\frac{\gamma}{k} \lesssim 1, \quad 2\sqrt{bk} + \gamma \ll 1, \quad \left(\frac{b}{k}\right)^{1/4} \ll 1. \quad (\text{S3})$$

Here and throughout we use $X \ll Y$ to denote an asymptotic relationship where $X/Y \rightarrow 0$, and $X \lesssim Y$ to indicate a bound on the ratio from above. We write $X \sim Y$ to mean that $X \lesssim Y$ and $Y \lesssim X$, or to pick out a typical value depending on the context.

2. Asymptotic isometries in and out of equilibrium

The first step in coarse-graining U is to decide whether minimizers are “asymptotically isometric”, meaning not only that their strain $\varepsilon \rightarrow 0$ but also that their stretching energy is negligible in comparison with the others, i.e.,

$$U_{\text{stretch}} \ll U_{\text{bend}} + U_{\text{sub}} + U_{\text{surf}}. \quad (\text{S4})$$

This concept was put forth in the series of papers [6, 8–10] culminating with the identification of the “Gauss-Euler

elastica” variational principle in [10] which here reads

$$\begin{aligned} \min \quad & U_{\text{bend}} + U_{\text{sub}} + U_{\text{surf}} \\ \text{subject to} \quad & U_{\text{stretch}} \ll U_{\text{bend}} + U_{\text{sub}} + U_{\text{surf}}. \end{aligned} \quad (\text{S5})$$

As it will help to motivate the way in which we coarse-grain, we pause to discuss how the existence of such an “asymptotically isometric regime” where minimizers satisfy (S4) can be deduced, permitting a proof that (S5) indeed captures the leading order behavior of ground and near ground states. The reader familiar with the subject may still wish to read on, as here we introduce a general approach for answering a key question highlighted in [10]:

Our analysis assumes that the minimal FvK energy can be safely evaluated through the upper bound obtained by solving the [Inverted Tension Field Theory] equations... Notwithstanding the agreement between our simulations and solutions of the ITFT eqs. we emphasize that the validity of the [Gauss-Euler elastica] rule hinges on the validity of this central assumption, which awaits a rigorous mathematical proof.

Finding a proof of the Gauss-Euler elastica is one of our main goals. Ultimately, our answer will be that it can be

established in a certain parameter regime without reference to the details of the patterns it predicts. We summarize the relevant issues now.

If the direction of wrinkling is considered known (say, due to symmetry) the required separation of energy scales (S4) can be connected to the original parameters through the use of “Inverted Tension Field Theory” [10], an asymptotic theory built for describing wrinkle patterns in the case of very weak tension $\gamma_{\text{lv}} \ll 2\sqrt{BK} \approx \gamma_{\text{eff}}$ and when $KR^2 \gg Y$ (small deformability, i.e., $k \gg 1$). Following the reasoning there one expects, at least in the ordered part of the shell, for the stress to be relaxed from its bare value $\sim \sigma_{\text{geom}} = YW^2/R^2$ down to a residual value $\sim \gamma_{\text{eff}}$ ignoring logarithmic corrections, in which case the stretching energy per unit area $u_{\text{stretch}} \sim \gamma_{\text{eff}}^2/Y$ while the remaining energies $u_{\text{bend}} + u_{\text{sub}} + u_{\text{surf}} \sim \gamma_{\text{eff}}W^2/R^2$. Since $\gamma_{\text{eff}} \ll \sigma_{\text{geom}}$ in the regime (S3), one predicts minimizers to be asymptotically isometric so that the formidable task of coarse-graining U should be equivalent to coarse-graining the Gauss-Euler elastica (S5). If, however, one is interested in deducing patterns this reasoning cannot be applied, as it requires *a priori* knowledge of optimizers. And although symmetry is sometimes a useful guide, notably even some initially axially symmetric shells exhibit a totally disordered response (see the positively curved discs in Figure 2 of the main text). Evidently, one needs a pattern-independent method of coarse-graining to predict the emergence of patterns.

The remainder of this section outlines our approach to coarse-graining U . The reader interested mainly in learning how to solve the maximum coverage problem that results can safely skip this discussion and go directly to Section III B (we do, however, recommend reading the summary of what is proved on page S8). We start by going one step beyond [10] and positing the existence of a “global asymptotic isometry regime” in which *any* possible state of effective tension-free strain

$$\varepsilon_{\text{eff}}(x) := e(u_{\text{eff}}) + \frac{1}{2}\nabla w_{\text{eff}} \otimes \nabla w_{\text{eff}} - \frac{1}{2}M \leq 0 \quad (\text{S6})$$

associated with *any* possible leading order displacement $(u_{\text{eff}}, w_{\text{eff}})$ can be recovered by an asymptotically isometric “recovery sequence” $(u, w) \rightarrow (u_{\text{eff}}, w_{\text{eff}})$ minimizing energy to leading order amongst all sequences converging to the effective state. The notion of “effective strain” in (S6) is natural as it indicates the strain that must be alleviated by the development of wrinkles or some other pattern. In essence, the global asymptotic isometry regime keeps track of when optimal patterns adapted to arbitrary tension-free ε_{eff} satisfy (S4). This is evidently more difficult to ascertain than the previous asymptotically isometric regime, which only requires minimizers to be asymptotically isometric. However, the introduction of such a globally defined regime will permit a global analysis of patterns both in and out of equilibrium, allowing us to deduce the validity of the Gauss-Euler elastica (S5) and to derive optimal patterns without *a priori* knowledge of their form. This passage from ground states to general states is the first key idea in our approach.

It is of course reasonable to ask whether the global asymptotic isometry regime exists. The arguments from [1] prove that it does under the following further (presumably technical) hypotheses: the planform is “strictly star-shaped” in that it admits an origin $x \in \Omega$ from which any $y \in \partial\Omega$ can be reached by a ray not leaving Ω ; the initial profile of the shell has second derivatives $\nabla\nabla p$ bounded in mean-square, i.e., $\int_{\Omega} |\nabla\nabla p|^2 < \infty$; and finally there holds in addition to (S3) the extra parameter restriction

$$\left(\frac{b}{k}\right)^{1/10} \ll 2\sqrt{bk} + \gamma \quad (\text{S7})$$

which in dimensional terms states that $\sigma_{\text{geom}} \ll N\gamma_{\text{eff}}$ where $N := (W/\lambda_{\text{sub}})^{2/5} \gg 1$. This is non-vacuous due to our initial hypothesis that $\gamma_{\text{eff}} \ll \sigma_{\text{geom}}$ in (S3). Under these additional hypotheses, [1, Sect. 3] constructs an asymptotically isometric recovery sequence for each $\varepsilon_{\text{eff}} \leq 0$, using a “piecewise herringbone” pattern built by tiling the shell with a large number $\sim N$ of individually herringboned squares. (Although the construction in [1] is written out for $w_{\text{eff}} = 0$, it can be altered to handle non-planar deformations as well. More on this later.) Herringbones are a familiar example of a two-scale wrinkling pattern which are known to be efficient at accomodating constant bi-axial compression [11, 12]. Our point is that by gluing many herringbones together, one can accommodate arbitrary tension-free ε_{eff} while driving the bare stress $\sim \sigma_{\text{geom}}$ down to a residual value estimated as $\lesssim N^{-1/2}\sigma_{\text{geom}} := \sigma_{\text{p.h.}}$ in the worst case. When $\sigma_{\text{geom}} \ll N\gamma_{\text{eff}}$ the piecewise herringbone pattern suffices to verify the global asymptotic isometry regime. Whether or not general asymptotically isometric recovery sequences exist when $\sigma_{\text{geom}} \gtrsim N\gamma_{\text{eff}}$ is presently open.

3. Derivation of the maximum coverage problem

We now expand the energy to leading order in the effective tension

$$\gamma_{\text{eff}} = 2\sqrt{BK} + \gamma_{\text{lv}} \rightarrow 0$$

in the global asymptotic isometry regime just introduced. In particular, we work in a limit where both (S3) and (S7) hold. In such a limit we claim that

$$U \stackrel{\Gamma}{=} \begin{cases} \gamma_{\text{eff}}\Delta A & \varepsilon_{\text{eff}} \leq 0, w_{\text{eff}} = 0 \\ \infty & \text{otherwise} \end{cases} + \text{h.o.t.} \quad (\text{S8})$$

when $\gamma \ll k$, which holds for a highly stiff substrate, and

$$U \stackrel{\Gamma}{=} \begin{cases} \gamma_{\text{eff}}\Delta A + \frac{K}{2} \int_{\Omega} |w_{\text{eff}}|^2 dx & \varepsilon_{\text{eff}} \leq 0 \\ \infty & \text{otherwise} \end{cases} + \text{h.o.t.} \quad (\text{S9})$$

when $\gamma \sim k$, which holds for a moderately stiff substrate. The symbol ∞ reflects an energy level significantly larger than the alternative while Γ refers to Γ -convergence, a

pattern-independent technique for coarse-graining to be introduced. The areal change

$$\Delta A = A_{\text{init}} - A_{\text{proj}} = \int_{\Omega} \frac{1}{2} \text{tr} M dx - \int_{\partial\Omega} u_{\text{eff}} \cdot \hat{v} ds \quad (\text{S10})$$

records the difference between the initial area of the shell and that of its deformed planform to leading order in the misfit $M = \nabla p \otimes \nabla p$ and displacement $u \approx u_{\text{eff}}$. The effective strain ε_{eff} is given in (S6). After obtaining the expansions (S8) and (S9) and checking the validity of the Gauss-Euler elastica (S5), we explain in a final step how minimization drives $w \rightarrow 0$ regardless of whether $\gamma \ll k$ or $\sim k$. The maximum coverage problem follows.

Let us pause for a moment to address the symbol Γ appearing above. It indicates a particular sense of coarse-graining built for non-convex minimization known as Γ -convergence. Standard references include [13, 14]; see also the introduction of [1]. Conceptually, it arises from finding the largest asymptotic lower bound U_{eff} on the energy U , with the idea being that such a lower bound

$$U \geq U_{\text{eff}} + \text{h.o.t.}$$

must “hug” the wells of U closely enough to coarse-grain. When combined with a so-called compactness result ensuring the abstract existence of effective states (achieved for effectively planar shells in [1, Sect. 2]), coarse-graining by Γ -convergence guarantees the following key results:

(i) the minimum energy expands as

$$\min U = \min U_{\text{eff}} + \text{h.o.t.}$$

in the relevant small parameters;

$$\frac{B}{2} |\Delta w|^2 + \frac{K}{2} |w|^2 = \sqrt{BK} (|\nabla w|^2 - \text{div}(w \nabla w)) + \frac{1}{2} \left| \sqrt{B} \Delta w + \sqrt{K} w \right|^2$$

yields the inequality

$$U_{\text{bend}} + U_{\text{sub}} \geq 2\sqrt{BK} \int_{\Omega} \frac{1}{2} |\nabla w|^2 + \text{h.o.t.} \quad (\text{S11})$$

after discarding non-negative, higher order, and other such harmless terms. Using (S1) to take the trace of the statement that $\varepsilon \rightarrow 0$ in any asymptotically isometric limit reveals the expansion

$$\int_{\Omega} \frac{1}{2} |\nabla w|^2 = \Delta A + \text{h.o.t.} \quad (\text{S12})$$

after applying (S10). Combining the previous two lines

(ii) any sequence of minimizers expands as

$$(u, w) = (u_{\text{eff}}, w_{\text{eff}}) + \text{h.o.t.}$$

where the effective state $(u_{\text{eff}}, w_{\text{eff}})$ minimizes U_{eff} .

The coarse-grained energy is identified as U_{eff} (its appropriately rescaled version is its “ Γ -limit”). Its minimizers consist not only of all possible limits of ground states, but also include limits of all possible “near ground states” with energy equal to the minimum at leading order. More generally, states $(u, w) \rightarrow (u_{\text{eff}}, w_{\text{eff}})$ satisfying

$$U = U_{\text{eff}} + \text{h.o.t.}$$

are distinguished as optimal to leading order amongst those consistent with the effective state. The existence of such “recovery sequences” is equivalent to U_{eff} being the largest possible asymptotic lower bound. The reader may note the terminology is consistent with the recovery sequences described in Section III A 2.

a. Highly stiff substrate ($\gamma \ll k$). We begin by establishing the expansion (S8). When the substrate is significantly stronger than the surface tension, the out-of-plane displacement $w \approx 0$. Indeed, any non-trivial effective out-of-plane displacement $w_{\text{eff}} \neq 0$ produces substrate energy per unit area $u_{\text{sub}} \gtrsim KW^4/R^2$. This is significantly larger than the anticipated $u_{\text{eff}} \sim \gamma_{\text{eff}} W^2/R^2$ when $\gamma \ll k$ and so can be ruled out. It is similarly straightforward to understand why $\varepsilon_{\text{eff}} \leq 0$, since if the limit fails to be tension-free there must be stress $\gtrsim \sigma_{\text{geom}} \gg \gamma_{\text{eff}}$ according to (S3).

The primary task is to expand the energy U of states $(u, w) \rightarrow (u_{\text{eff}}, 0)$ with $\varepsilon_{\text{eff}} \leq 0$. Of course there are many such sequences but, as we are coarse-graining by Γ -convergence, we shall only treat those making U as low as possible for the given effective state. First, we estimate U from below. Integrating the calculus identity

(S11) and (S12) with the definition of the effective tension $\gamma_{\text{eff}} = 2\sqrt{BK} + \gamma_{\text{lv}}$ produces the lower bound

$$U \geq \gamma_{\text{eff}} \Delta A + \text{h.o.t.} \quad (\text{S13})$$

regardless of how $(u, w) \rightarrow (u_{\text{eff}}, 0)$.

Of course, the true energy U of a more or less arbitrary state $(u, w) \approx (u_{\text{eff}}, 0)$ may be much larger than the lower

bound $\gamma_{\text{eff}}\Delta A$ just established. Nevertheless, an optimal piecewise herringbone pattern defines an asymptotically isometric recovery sequence $(u, w) \rightarrow (u_{\text{eff}}, 0)$ for each $\varepsilon_{\text{eff}} \leq 0$, meaning here that its energy satisfies

$$U = \gamma_{\text{eff}}\Delta A + \text{h.o.t.}$$

This verifies optimality of the lower bound (S13) and establishes the expansion (S8). That the sequence is asymptotically isometric is readily checked using the estimates from [1]. Its stretching energy per unit area obeys $u_{\text{stretch}} \lesssim \sigma_{\text{p.h.}}^2/Y$, where $\sigma_{\text{p.h.}} = N^{-1/2}\sigma_{\text{geom}}$ is a worst case estimate of its stress. The hypothesis (S7) ensures this is negligible as compared with the remaining terms $u_{\text{bend}} + u_{\text{sub}} + u_{\text{surf}} \sim \gamma_{\text{eff}}W^2/R^2$. See [1, Sect. 3] for the estimates and [1, Sect. 2] for more on the lower bound.

b. Moderately stiff substrate ($\gamma \sim k$). When substrate and surface tension forces are comparable the expansion (S9) applies for reasons we explain now. The same argument as before shows that $\varepsilon_{\text{eff}} \leq 0$, as if the limit is not tension-free there must arise a stress $\gtrsim \sigma_{\text{geom}} \gg \gamma_{\text{eff}}$ as well as KW^2 due to (S3) and the condition of a moderately stiff substrate.

Continuing, we note that $2\sqrt{BK} \ll \gamma_{\text{lv}} \approx \gamma_{\text{eff}}$ throughout the present regime. So, to expand the energy of states $(u, w) \rightarrow (u_{\text{eff}}, w_{\text{eff}})$ it will be enough to keep track of the substrate and surface terms. These satisfy

$$U_{\text{sub}} = \frac{K}{2} \int_{\Omega} |w_{\text{eff}}|^2 + \text{h.o.t.} \quad \text{and} \quad U_{\text{surf}} = \gamma_{\text{lv}}\Delta A + \text{h.o.t.}$$

and therefore

$$U \geq \gamma_{\text{lv}}\Delta A + \frac{K}{2} \int_{\Omega} |w_{\text{eff}}|^2 + \text{h.o.t.} \quad (\text{S14})$$

for general states $(u, w) \rightarrow (u_{\text{eff}}, w_{\text{eff}})$. That the bound is optimal can again be checked using a piecewise herringbone to perturb about tension-free $(u_{\text{eff}}, w_{\text{eff}})$. We emphasize that the out-of-plane part w_{eff} need not vanish at this step, even if eventually upon minimization it does. As this possibility is not treated explicitly in [1], we explain how to build the required perturbation.

Define the in- and out-of-plane displacements

$$u = u_{\text{eff}} - \xi_{\text{p.h.}} \nabla w_{\text{eff}} + v_{\text{p.h.}} \quad \text{and} \quad w = w_{\text{eff}} + \xi_{\text{p.h.}}$$

where the oscillatory variables $v_{\text{p.h.}}$ and $\xi_{\text{p.h.}}$ describe an optimal piecewise herringbone. The estimates in [1, Sect. 3] then show that the resulting strain

$$\varepsilon = e(v_{\text{p.h.}}) + \frac{1}{2} \nabla \xi_{\text{p.h.}} \otimes \nabla \xi_{\text{p.h.}} - \xi_{\text{p.h.}} \nabla \nabla w_{\text{eff}} - (-\varepsilon_{\text{eff}}) \rightarrow 0.$$

The stretching energy per unit area $u_{\text{stretch}} \lesssim \sigma_{\text{p.h.}}^2/Y$ with stress $\lesssim \sigma_{\text{p.h.}} = N^{-1/2}\sigma_{\text{geom}}$ as before. The term $\sim \xi_{\text{p.h.}} \nabla \nabla w_{\text{p.h.}}$ enters at higher order. The bending energy $u_{\text{bend}} \sim \sqrt{BK}W^2/R^2$, while the remaining terms $u_{\text{sub}} + u_{\text{surf}} \sim (KW^2 + \gamma_{\text{lv}})W^2/R^2$. Both stretching and bending are negligible as anticipated (here we use (S7) to

control u_{stretch}). Hence, the perturbation is asymptotically isometric with energy

$$U = \gamma_{\text{lv}}\Delta A + \frac{K}{2} \int_{\Omega} |w_{\text{eff}}|^2 + \text{h.o.t.}$$

indicating it is a recovery sequence. The lower bound (S14) is optimal and the expansion (S9) is proved.

c. The maximum coverage problem. All that remains is to show that minimizing the leading order terms in (S8) and (S9) drives $w \rightarrow 0$. In fact, we only need to check that this holds for a moderately stiff substrate ($\gamma \sim k$) since $w_{\text{eff}} = 0$ appears already as a constraint in (S8). So, we consider the coarse-grained problem

$$\min_{\substack{u_{\text{eff}}(x), w_{\text{eff}}(x) \\ \varepsilon_{\text{eff}} \leq 0}} \gamma_{\text{eff}}\Delta A(u_{\text{eff}}) + \frac{K}{2} \int_{\Omega} |w_{\text{eff}}|^2 \quad (\text{S15})$$

implied by (S9). If an admissible tension-free $(u_{\text{eff}}, w_{\text{eff}})$ has some non-trivial out-of-plane part, then the projected displacement $(u_{\text{eff}}, 0)$ is both tension-free with

$$\varepsilon_{\text{eff}} = e(u_{\text{eff}}) - \frac{1}{2}M \leq e(u_{\text{eff}}) + \frac{1}{2}\nabla w_{\text{eff}} \otimes \nabla w_{\text{eff}} - \frac{1}{2}M \leq 0$$

and obtains the strictly smaller coarse-grained energy

$$U_{\text{eff}} = \gamma_{\text{eff}}\Delta A < \gamma_{\text{eff}}\Delta A + \frac{K}{2} \int_{\Omega} |w_{\text{eff}}|^2.$$

Therefore, solutions of (S15) must have $w_{\text{eff}} = 0$ and the maximum coverage principle is proved.

Summary. We have shown in a pattern-independent coarse-graining by Γ -convergence that (i) any sequence of ground or near ground states $(u, w) \rightarrow (u_{\text{eff}}, w_{\text{eff}})$ satisfies

$$U \approx \gamma_{\text{eff}}\Delta A, \quad \varepsilon_{\text{eff}} \leq 0, \quad \text{and} \quad w_{\text{eff}} = 0$$

where u_{eff} achieves maximum coverage minimizing the areal change $\Delta A = A_{\text{init}} - A_{\text{proj}}$ amongst all tension-free effective states and, moreover, (ii) all solutions of the maximum coverage problem arise as limits of near ground states having minimal energy at leading order. Implicit in our argument was a proof that the Gauss-Euler elastica (S5) yields a correct leading order description of ground and near ground states.

Due to our use of piecewise herringbones to construct nearly optimal perturbations about an *a priori* unknown effective state, these results are only presently known to hold under the further technical hypotheses in the paragraph around (S7) beyond the initial regime (S3). This is with the notable exception of the case of a negatively curved disc, whereupon combining the results of [10] with our solution of the maximum coverage problem to follow, we can conclude the validity of (i) and (ii) in the part of (S3) having very weak tension $\gamma_{\text{lv}} \ll 2\sqrt{BK}$ and a strong substrate $KR^2 \gg Y$ up to logarithmic corrections. We wonder exactly to what extent the Gauss-Euler elastica and maximum coverage problem predict the patterns formed by confined elastic shells.

B. Highly wrinkled shells as ideal locking materials

The previous section explained how the maximum coverage problem

$$\min_{\substack{u_{\text{eff}}(x) \\ \varepsilon_{\text{eff}} \leq 0}} \Delta A \quad (\text{S16})$$

arises from coarse-graining the energy U . There, we explained under suitable hypotheses how the displacements $(u, w) \rightarrow (u_{\text{eff}}, 0)$ while alleviating whatever effective strain $\varepsilon_{\text{eff}} = e(u_{\text{eff}}) - \frac{1}{2}M$ develops. Naturally, to determine the effective in-plane displacement u_{eff} one can consider minimizing its implied energetic cost $\approx \gamma_{\text{eff}} \Delta A$, and this is precisely what (S16) is asking to do. The

The out-of-plane displacement w of any ground or near ground state obeys

$$w(x) \approx \text{a function of } x \cdot \hat{T}^\perp(x) \quad \text{where the locking stress } \sigma_L(x) \sim \hat{T}(x) \otimes \hat{T}(x). \quad (\text{S17})$$

The unit vector field $\hat{T}(x)$ denotes a principal direction of positive locking stress. We call curves passing parallel to it “stable lines”. Of course, this conclusion is contingent upon the statement that the maximum coverage problem governs the effective displacement of the shell (this was the subject of Section III A). In any case, one may always try to plot the stable lines of a shell to see what they predict, and this is exactly what we have done in Figures 1 and 2 of the main text.

1. The locking stress

The maximum coverage problem (S16) is a constrained optimization taking in only those displacements $u_{\text{eff}}(x)$ for which $\varepsilon_{\text{eff}}(x) \leq 0$. Rather than solving it directly, we instead invoke a Lagrange multiplier formulation with the goal of solving for the multiplier first. It will turn out to be the anticipated locking stress $\sigma_L(x)$ whose structure reveals that of the effective strain.

The first step is to introduce a Lagrange multiplier for the tension-free constraint. Observe that

$$\varepsilon_{\text{eff}}(x) \leq 0 \iff \int_{\Omega} \sigma_L : \varepsilon_{\text{eff}} \leq 0 \quad \text{for all } \sigma_L(x) \geq 0,$$

meaning that the given ε_{eff} is tension-free exactly when its integral against σ_L is non-positive for all non-negative two-by-two symmetric tensors (not yet the locking stress). With this, we can rewrite the maximum coverage problem in its Lagrange multiplier form

$$\min_{\substack{u_{\text{eff}}(x) \\ \varepsilon_{\text{eff}} \leq 0}} \Delta A = \min_{u_{\text{eff}}(x)} \max_{\substack{\sigma_L(x) \\ \sigma_L \geq 0}} \mathcal{L}$$

using the Lagrangian

$$\mathcal{L} = \Delta A + \int_{\Omega} \sigma_L : \varepsilon_{\text{eff}}.$$

remainder of this supplementary text offers an in depth look at how to solve the maximum coverage problem for general planforms Ω and misfits $M(x)$.

We begin by introducing a tensor dual to the effective strain called the “locking stress” $\sigma_L(x)$. Our idea is simple: a highly wrinkled shell should behave as one of Prager’s ideal locking materials [15] since its effective strain must remain tension-free (≤ 0). As such, it should admit a locking stress whose structure reflects that of the effective strain, whence the patterns. We start in Section III B 1 by producing a variational principle for σ_L . Section III B 2 derives its first order optimality conditions resulting in the crucial orthogonality of σ_L and ε_{eff} . Using it, we introduce our method of stable lines in Section III B 3, the primary conclusion of which is as follows:

The min-max problem indeed recovers the maximum coverage one, since if u_{eff} admits some σ_L for which the integral is > 0 , then by scaling its amplitude we can drive the max $\rightarrow +\infty$. The role of the maximization is nothing other than to enforce the tension-free constraint.

Now the key point: by switching the order of operations between min and max we can identify the dual locking stress problem for σ_L . To prepare, note by the formula (S10) for the areal change that

$$\begin{aligned} \mathcal{L} &= \int_{\Omega} (\sigma_L - Id) : \varepsilon_{\text{eff}} \\ &= -\frac{1}{2} \int_{\Omega} (\sigma_L - Id) : M + \int_{\Omega} (\sigma_L - Id) : e(u_{\text{eff}}), \end{aligned} \quad (\text{S18})$$

where the last term can be rewritten using the divergence theorem as

$$\begin{aligned} &\int_{\Omega} (\sigma_L - Id) : e(u_{\text{eff}}) \\ &= - \int_{\Omega} \operatorname{div} \sigma_L \cdot u_{\text{eff}} + \int_{\partial\Omega} (\sigma_L - Id) \hat{\nu} \cdot u_{\text{eff}} ds. \end{aligned} \quad (\text{S19})$$

Minimizing the righthand side amongst all u_{eff} , we see it is possible to drive it $\rightarrow -\infty$ unless

$$\operatorname{div} \sigma_L = 0 \text{ in } \Omega \quad \text{and} \quad \sigma_L \hat{\nu} = \hat{\nu} \text{ at } \partial\Omega \quad (\text{S20})$$

in which case it vanishes regardless of u_{eff} . It follows by the same reasoning as before that

$$\max_{\substack{\sigma_L(x) \\ \sigma_L \geq 0}} \min_{u_{\text{eff}}(x)} \mathcal{L} = \max_{\substack{\sigma_L(x) \geq 0 \\ \operatorname{div} \sigma_L = 0 \text{ in } \Omega \\ \sigma_L \hat{\nu} = \hat{\nu} \text{ at } \partial\Omega}} -\frac{1}{2} \int_{\Omega} (\sigma_L - Id) : M$$

yielding the desired locking stress problem on the right. Its solution, when it exists, defines the locking stress $\sigma_L(x)$ of an effectively planar shell.

A few words are in order on the relation between the maximum coverage (min-max) and locking stress problem (max-min) just derived. First, on the claimed duality between the two, we note that indeed

$$\min_{\substack{u_{\text{eff}}(x) \\ \varepsilon_{\text{eff}} \leq 0}} \Delta A = \max_{\substack{\sigma_L(x) \geq 0 \\ \text{div } \sigma_L = 0 \text{ in } \Omega \\ \sigma_L \hat{\nu} = \hat{\nu} \text{ at } \partial\Omega}} -\frac{1}{2} \int_{\Omega} (\sigma_L - Id) : M \quad (\text{S21})$$

both in the literal sense that their optimal values are the same, as well as in the sense that there is a correspondence between solutions ε_{eff} and σ_L . Unfortunately, the formal “minimax” argument given above does not suffice to conclude (S21), as without further structural hypotheses on the Lagrangian only $\min \max \mathcal{L} \geq \max \min \mathcal{L}$ holds. In the present context, however, we can appeal to the bilinearity of \mathcal{L} to apply one of various “minimax theorems” showing that $\min \max \mathcal{L} = \max \min \mathcal{L}$ (we use the one by Fenchel and Rockafeller in [1, Sect. 4]). This proves the duality (S21). Its importance manifests in the orthogonality relation it implies between solutions ε_{eff} and σ_L , which we derive in Section III B 2 and again in Section III C 1 in an Airy potential formulation.

Second, on the existence of optimizers and the definition of locking stress, we point out that the situation is more subtle than one might initially suspect. While tension-free u_{eff} minimizing ΔA do always exist, there are simple counterexamples (e.g., positively curved discs) in which no admissible σ_L attains the maximum in (S21). This is due to the following phenomena: a “maximizing sequence” driving the integral up to its largest value can (i) exhibit a loss of the ill-posed boundary condition $\sigma_L \hat{\nu} = \hat{\nu}$, and (ii) develop singular behavior wherein σ_L concentrates along curves. In the example of the positively curved disc both situations occur (every such sequence tends to zero in its interior while concentrating as $r \hat{e}_{\theta} \otimes \hat{e}_{\theta}$ at its boundary). Fortunately, as established in [1, Sect. 4], locking stresses can always be defined as *limits* of maximizing sequences. Rather than dwell on this further, we refer the interested reader to the reference and instead prefer to keep the discussion as intuitive as possible by simply speaking of $\sigma_L(x)$ as a “solution” of the locking stress problem. The reader wishing to see a well-posed version for which maximizers are directly guaranteed to exist should read on to Section III C 1 where the offending boundary condition is relaxed.

2. Orthogonality of stress and strain

We proceed to derive the orthogonality of the locking stress σ_L and effective strain ε_{eff} . As will become clear in the pending discussion of stable lines, this is the key to understanding the layout of the patterns. Whereas general admissible σ_L and ε_{eff} satisfy

$$\Delta A \geq -\frac{1}{2} \int_{\Omega} (\sigma_L - Id) : M, \quad (\text{S22})$$

optimizers can be identified with the case of equality due to (S21). A direct proof of (S22) can be given revealing the desired relation. Rearranging (S18) and applying the admissibility criteria (S20) we find that

$$\Delta A + \frac{1}{2} \int_{\Omega} (\sigma_L - Id) : M = \int_{\Omega} |\sigma_L : \varepsilon_{\text{eff}}| \geq 0$$

where the absolute value comes from known signs. Thus, admissible ε_{eff} and σ_L are optimal if and only if

$$\sigma_L : \varepsilon_{\text{eff}} = 0 \quad \text{in } \Omega. \quad (\text{S23})$$

This sort of orthogonality condition is known as “complementary slackness” in convex duality. It plays the role of the Euler-Lagrange equations for the (constrained) maximum coverage and locking stress problems.

Although such orthogonality may seem strange from a Hookean point of view, it is consistent with the modeling of ideal locking materials initiated by Prager as a theoretical possibility opposite to perfect elasto-plasticity [15]. A similar orthogonality arises in the Lagrangian treatment of constraining forces (e.g., bead on a hoop), and indeed σ_L was introduced as a Lagrange multiplier. We proceed to its use for determining wrinkle patterns.

3. The method of stable lines

The facts just derived regarding the locking stress σ_L and effective strain $\varepsilon_{\text{eff}} = e(u_{\text{eff}}) - \frac{1}{2}M$ set serious restrictions on the patterns. At the most basic level, where one is of full rank the other must vanish as they are orthogonal. Where σ_L is of full rank, $\varepsilon_{\text{eff}} = 0$ but this is impossible where the misfit is incompatible, i.e., where $\kappa = -\frac{1}{2} \text{curlcurl } M \neq 0$. It is, of course, entirely possible that the ranks of σ_L and ε_{eff} are both one, and this is the situation where wrinkles or some other locally one-dimensional pattern occurs. It is also possible that ε_{eff} be of full rank so that $\sigma_L = 0$; the converse is, however, less clear as just because σ_L vanishes it does not necessarily imply that a two-dimensional pattern must form.

Nevertheless, we refer to the portion of the shell where $\sigma_L = 0$ as “disordered” as that is where the experiments and simulations exhibit a generically statistical response. Likewise, we refer to the portion where $\sigma_L \neq 0$ as “ordered”, since there patterns are locally one-dimensional with peaks and troughs approximating curves we call “stable lines” — curves passing by definition through the principal direction of positive σ_L . Where σ_L is smooth stable lines must remain straight. Where it is singular, their direction can sharply change.

To explain all this in more detail we start by noting that in any asymptotically isometric limit where, necessarily, $\varepsilon \rightarrow 0$ the approximation

$$\frac{1}{2} \nabla w \otimes \nabla w \approx \frac{1}{2} M - e(u)$$

holds to leading order by (S1). Taking the inner product against the locking stress yields

$$\sigma_L : \frac{1}{2} \nabla w \otimes \nabla w \approx \sigma_L : \left(\frac{1}{2} M - e(u) \right) \rightarrow \sigma_L : -\varepsilon_{\text{eff}}$$

since $e(u) \rightarrow e(u_{\text{eff}})$ and we are working in a limit where $w_{\text{eff}} = 0$. The inner product on the right vanishes due to the orthogonality relation (S23). Thus,

$$\sigma_L : \nabla w \otimes \nabla w \rightarrow 0. \quad (\text{S24})$$

Now suppose $\hat{T}(x)$ is a principal direction of positive locking stress, meaning that $\sigma_L(x) \sim \hat{T}(x) \otimes \hat{T}(x)$. Setting this into (S24) shows that $\hat{T} \cdot \nabla w \rightarrow 0$. In other words,

$$w(x) \approx \text{a function of } x \cdot \hat{T}^\perp(x)$$

exactly as asserted in (S17). Leading order deviations to this rule cost significant amounts of energy, so we think of it as an asymptotically stabilizing effect.

We complete the present discussion by deriving a general classification scheme for wrinkle patterns via their stable lines. First, we explain why any curve parallel to a principal direction of positive σ_L must be straight. Locally, at least, an Airy potential φ can be introduced solving $\sigma_L = \nabla^\perp \nabla^\perp \varphi$. Where σ_L is rank one, $\det \nabla \nabla \varphi = 0$. It follows that the graph of φ describes a developable surface, i.e., one whose Gaussian curvature vanishes identically and is made up of ruling lines [16, 17]. Projecting these to the plane yields the stable lines. Pursuing this one step further, we note that there are exactly three classes of smooth, non-planar developable surfaces, given by cylinders, cones, and tangential developables (with ruling lines tangent to a space curve). Upon projection we recover the analogous three classes of stable lines. We turn to explain how the solution of σ_L can be simplified by the introduction of an Airy potential in the large.

C. Solution of the locking stress problem for simply connected shells

The previous section derived the locking stress problem

$$\max_{\substack{\sigma_L(x) \geq 0 \\ \text{div } \sigma_L = 0 \text{ in } \Omega \\ \sigma_L \hat{\nu} = \hat{\nu} \text{ at } \partial\Omega}} -\frac{1}{2} \int_{\Omega} (\sigma_L - Id) : M \quad (\text{S25})$$

as dual to the maximum coverage one (S16). Together, these govern the leading order features of effectively planar shells. Locking stresses are, however, in general only defined as *limits* of maximizing sequences due to the ill-posed boundary condition $\sigma_L \hat{\nu} = \hat{\nu}$. This procedure can

often be difficult to implement in practice, so here we consider the possibility of passing to a “relaxed” formulation in which maximizers are directly defined.

Section III C 1 derives the relaxed locking stress problem for simply connected shells (lacking holes), using a change of variables from $\sigma_L(x)$ to a class of Airy potentials $\varphi(x)$. Following this, we discuss various techniques for producing optimal φ in Section III C 2 and Section III C 3. The methods we describe are generally appropriate when the Gaussian curvature $\kappa(x)$ is either everywhere positive or negative. The reader may note that each of the examples appearing in Figures 1-3 of the main text verify these constraints — see, however, the discussion around Figure 4a,b for relevant questions.

1. The relaxed Airy potential formulation

Introduce an Airy potential $\varphi(x)$ by setting

$$\sigma_L = \nabla^\perp \nabla^\perp \varphi = \begin{pmatrix} \partial_{22} & -\partial_{12} \\ -\partial_{12} & \partial_{11} \end{pmatrix} \varphi$$

into the locking stress problem (S25). Boundary conditions must be determined that are both general enough to guarantee the existence of optimizing φ , while not so general that their relation with σ_L is lost. Due to our assumption that the shell is simply connected, it will turn out to be appropriate to enforce that

$$\varphi = \frac{1}{2} |x|^2 \quad \text{and} \quad \hat{\nu} \cdot \nabla \varphi \leq \hat{\nu} \cdot x \quad \text{at } \partial\Omega. \quad (\text{S26})$$

Note the inequality permits possible singular behavior in the boundary values of the locking stress, associated with the loss of the ill-posed boundary condition $\sigma_L \hat{\nu} = \hat{\nu}$ anticipated in Section III B 1. Of course, we must still have that $\sigma_L \geq 0$ throughout, and hence $\nabla \nabla \varphi \geq 0$ equivalent to the local convexity of φ . The boundary conditions (S26) facilitate extending φ to the plane by setting it equal to $\frac{1}{2} |x|^2$ outside Ω . The result is that we can simply require it to be convex in the usual sense, i.e.,

$$\varphi(\theta x + (1 - \theta)y) \leq \theta \varphi(x) + (1 - \theta) \varphi(y)$$

whenever $x, y \in \mathbb{R}^2$ and $0 \leq \theta \leq 1$. Thus we relax the initial set of admissible σ_L in the ill-posed formulation (S25) to the strictly larger set generated by convex extensions φ of $\frac{1}{2} |x|^2$ into Ω . We claim now that this captures all possible locking stresses of simply connected shells.

The crux of the matter is to show that optimizing over σ_L following (S25) produces the same maximum as optimizing over the admissible φ just defined. That is, we seek the equality

$$\max_{\substack{\sigma_L(x) \geq 0 \\ \operatorname{div} \sigma_L = 0 \text{ in } \Omega \\ \sigma_L \hat{\nu} = \hat{\nu} \text{ at } \partial\Omega}} -\frac{1}{2} \int_{\Omega} (\sigma_L - Id) : M = \max_{\substack{\varphi(x) \\ \varphi \text{ is convex} \\ \varphi = \frac{1}{2}|x|^2 \text{ outside } \Omega}} \int_{\Omega} \left(\varphi - \frac{1}{2}|x|^2 \right) \kappa \quad (\text{S27})$$

between the original ill-posed locking stress problem and its relaxed Airy potential formulation on the right. Let us highlight the main points now. Since $\kappa = -\frac{1}{2}\operatorname{curlcurl} M$, an integration by parts shows that

$$-\frac{1}{2} \int_{\Omega} (\sigma_L - Id) : M = \int_{\Omega} \left(\varphi - \frac{1}{2}|x|^2 \right) \kappa$$

so long as equality holds in *both* parts of (S26). This is the case for the initial admissible σ_L , and as maximizing over a more general class never decreases the result the maximum on the right of (S27) is at least as large as the one on the left. An integration by parts using the relaxed boundary conditions (S26) shows the opposite inequality holds. Together, these yield (S27). Existence of an optimal φ is guaranteed by the so-called direct method of the calculus of variations; see [1, Sect. 4] for the details.

The Airy potential formulation of the locking stress problem just derived has many advantages over the original one. Not only does it always possess a solution $\varphi(x)$ thereby allowing to directly compute the locking stress, its form makes explicit the role of the sign of the curvature $\kappa(x)$ and this is the focus of Section III C 2 and Section III C 3. First, however, we produce the relaxed version of the crucial orthogonality relation (S23) between the locking stress and effective strain.

Optimality of ε_{eff} and φ is characterized as the case of equality in the general inequality

$$\Delta A \geq \int_{\Omega} \left(\varphi - \frac{1}{2}|x|^2 \right) \kappa$$

due to (S27). A similar integration by parts as underlies (S23) shows that

$$\begin{aligned} \Delta A - \int_{\Omega} \left(\varphi - \frac{1}{2}|x|^2 \right) \kappa &= \\ \frac{1}{2} \int_{\Omega} |\nabla^{\perp} \nabla^{\perp} \varphi : \varepsilon_{\text{eff}}| + \frac{1}{2} \int_{\partial\Omega} |\hat{\nu} \cdot (x - \nabla \varphi) (\varepsilon_{\text{eff}})_{\hat{\tau}\hat{\tau}}| &\geq 0 \end{aligned}$$

with absolute values coming from known signs. Hence, ε_{eff} and φ are optimal if and only if they satisfy the relaxed complementary slackness conditions

$$\begin{cases} \nabla^{\perp} \nabla^{\perp} \varphi : \varepsilon_{\text{eff}} = 0 & \text{in } \Omega \\ \hat{\nu} \cdot (x - \nabla \varphi) (\varepsilon_{\text{eff}})_{\hat{\tau}\hat{\tau}} = 0 & \text{at } \partial\Omega \end{cases}. \quad (\text{S28})$$

While we recognize the first condition as a rewrite of the orthogonality in (S23), the second condition is new and reflects a possible concentration of the locking stress at the boundary $\sim \hat{\nu} \cdot (x - \nabla \varphi) \hat{\tau} \otimes \hat{\tau}$ where $\hat{\nu}$ and $\hat{\tau}$ are the outwards pointing normal and tangent vectors. Keeping track of such singularities turns out to be crucial for recovering the displacements of certain (positively curved) shells. We return to this later on in Section III D.

2. Solutions and geometric constructions, positive curvature

Having passed to the relaxed Airy potential formulation of the problem, we turn to consider its solution for locking stresses and stable lines. Stable lines are always defined in the ordered region $\sigma_L = \nabla^{\perp} \nabla^{\perp} \varphi \neq 0$ as lines along which an optimal Airy potential $\varphi(x)$ is affine while in a transverse direction it is not. Indeed,

$$\nabla^{\perp} \nabla^{\perp} \varphi(x) \sim \hat{T} \otimes \hat{T}(x) \iff \partial_{\hat{T}}^2 \varphi(x) = 0, \partial_{\hat{T}^{\perp}}^2 \varphi(x) \neq 0$$

where $\hat{T}(x)$ denotes a principal direction of locking stress and $\partial_{\hat{T}} = \hat{T} \cdot \nabla$ a derivative along the stable lines. Disorder restricts to where $\varphi(x)$ is locally affine, as the locking stress $\sigma_L = \nabla^{\perp} \nabla^{\perp} \varphi = 0$ there.

There are two extreme cases in which an optimal Airy potential is most easily found: when the curvature $\kappa(x)$ is either everywhere positive, or when it is everywhere negative. Starting with the first case, we note that when $\kappa > 0$ producing the locking stress is equivalent to finding the largest convex extension φ_+ of $\frac{1}{2}|x|^2$ into Ω , i.e.,

$$\varphi_+(x) := \max \left\{ \varphi(x) : \varphi \text{ is a convex ext. of } \frac{1}{2}|x|^2 \right\}.$$

Indeed, this sets an upper bound on all other convex extensions while it is one itself. Thus, φ_+ is the unique maximizer of the integral on the righthand side of (S27). Note this holds even when $\kappa(x)$ is not constant so long as it is > 0 ; moreover, in the case that $\kappa(x)$ vanishes somewhere but is still ≥ 0 , φ_+ remains optimal.

Actually, it is not so difficult to determine the largest convex extension φ_+ so long as the planform Ω is reasonably defined. Consider, for instance, the class of shells with “tangential polygon” planforms $\Omega = P$ which, by definition, are polygons having an inscribed circle $C \subset P$. Define the points of tangency of C with ∂P to be the vertices of the planform’s “contact polygon”, P' . The contact polygon is precisely where $\sigma_L = \nabla^{\perp} \nabla^{\perp} \varphi_+ = 0$, and it is predicted to be (generically) disordered. Outside P' , φ_+ is affine upon restriction to line segments parallel to its sides: these are the stable lines predicting wrinkle peaks and troughs. The “inscribed circle” or “contact polygon” construction just described underlies several of the positively-curved predictions in Figures 1 and 2 of the main text. Representative stable lines are plotted in blue alongside contact polygons in white. Dotted blue lines reflect the important point that we neglect a small tensional rim when inscribing the circle C into P . A detailed study of this rim is the subject of ongoing work. For questions regarding its sensitivity to perturbations see Section III F.

Even if the planform is not a tangential polygon, it may still admit a family of maximally contained circles whose extremal ones set the response. This is the case, in particular, for a rectangle which admits a one-parameter family of maximal circles and two extremal ones towards its short sides. The associated contact polygons, with obvious definitions, have $\sigma_L = \nabla^\perp \nabla^\perp \varphi_+ = 0$ and the wrinkle pattern is recovered outside them by drawing stable lines parallel to their sides along which φ_+ is affine. Other, more general positively curved shells can be similarly solved, even if their patterns do not follow such simple inscribed/extremal circle rules. Looking back to Figure 2 in the text, we see that while the half-disc is tangential in that it admits an inscribed circle, the associated construction does *not* explain the wrinkle pattern that results — of course, the half-disc is not a polygon. Instead, circumscribing a circle and describing a polar coordinate system about a symmetrically disposed point on the “ghost” arc reveals the wrinkle direction and stable lines (parallel to the angular and radial directions, respectively). The same construction also applies to circular planforms with a strip removed, see Figure S3b.

In lieu of geometric intuition, one can always deduce the largest convex extension φ_+ by carrying out the following minimization routine: given $x \in \Omega$,

$$\varphi_+(x) = \min_{\{y_i\} \subset \partial\Omega} \sum_{i=1}^3 \theta_i \frac{1}{2} |y_i|^2 \quad (\text{S29})$$

over pairs and triples $\{y_i\} \subset \partial\Omega$ satisfying

$$x = \sum_i \theta_i y_i \quad \text{for } 0 < \theta_i < 1 \text{ and } \sum_i \theta_i = 1.$$

This describes an optimal partitioning of the shell into ordered and disordered parts. Figure S2 depicts three admissible partitions for a square with the optimal one on the far right. In an admissible partition, candidate stable lines fill out the candidate ordered part generated by points x described using pairs $\{y_i\}_{i=1}^2$. The leftover candidate disordered part is convex, being generated by points x described via triples $\{y_i\}_{i=1}^3$. Optimizing over all such partitions as per (S29) yields the true stable lines.

3. Solutions and geometric constructions, negative curvature

In the negatively curved case $\kappa(x) < 0$, it is the smallest convex extension $\varphi_-(x)$ of $\frac{1}{2}|x|^2$ that solves the locking stress problem setting the patterns. Indeed, any other extension is bounded below by

$$\varphi_-(x) := \min \left\{ \varphi(x) : \varphi \text{ is a convex ext. of } \frac{1}{2}|x|^2 \right\}$$

which is an admissible Airy potential itself. So, when the curvature is negative the integral on the righthand side of (S27) is maximized precisely by saturating this lower

bound. Again, this does not require $\kappa(x)$ to be constant but only to be < 0 ; φ_- is still optimal when it is ≤ 0 .

We now produce the locking stresses and stable lines of negatively curved shells. This time, there is a ubiquitous solution procedure independent of the simply connected planform Ω . It is conveniently encoded in the definition of the “boundary distance” function

$$d_{\partial\Omega}(x) := \min_{y \in \partial\Omega} |x - y|, \quad x \in \Omega$$

from which one obtains that

$$\varphi_-(x) = \frac{1}{2}|x|^2 - \frac{1}{2}d_{\partial\Omega}^2(x).$$

Differentiation yields the locking stress

$$\sigma_L = \nabla^\perp \nabla^\perp \varphi_- = (1 - d_{\partial\Omega} \Delta d_{\partial\Omega}) \nabla^\perp d_{\partial\Omega} \otimes \nabla^\perp d_{\partial\Omega}$$

in regions where the boundary distance function is smoothly defined. We note φ_- is affine along lines of closest approach of points $x \in \Omega$ to the boundary $\partial\Omega$, which are parallel to $\nabla d_{\partial\Omega}$. That is, the direction of steepest ascent of $d_{\partial\Omega}$ is a principal direction of positive σ_L and the lines of closest approach are the stable lines. They extend perpendicularly from the boundary of the planform and meet at its “medial axis” or “skeleton”

$$\{x \in \Omega : d_{\partial\Omega}(x) = |x - y| \text{ for multiple } y \in \partial\Omega\}.$$

There, $\nabla d_{\partial\Omega}$ is not defined and σ_L concentrates. Disorder is ruled out. We have thus arrived at the striking conclusion that wrinkles for negatively curved shells solve the famous minimum exit time problem, a problem familiar from optimal control theory and geometric optics.

These predictions for the wrinkle patterns of negatively curved shells are shown in the corresponding parts of Figures 1 and 2 of the main text. Similarly to the tensional rim in the positively curved case, we observe a larger tensional core for negatively curved shells. The core contains the medial axis in our experiments and simulations. Its size in a related radially symmetric setup was studied in [10, 18]. Here, we have produced a method for determining its general location and shape.

D. Recovering the effective strain and r.m.s. amplitude

Having developed the theory of locking stresses for effectively planar shells, we now return to the coarse-grained maximum coverage problem (S16) to show how the effective strain ε_{eff} and accompanying displacements can be recovered from knowledge of stable lines. The key concept put forth here is that of the “defect measure” $\mu(dx) := \langle \nabla w \otimes \nabla w \rangle$ of an elastic pattern. The angle brackets $\langle \cdot \rangle$ indicate a notion of asymptotic averaging over small scales to be made precise. Determining the defect measure of a pattern is the first step in approximating its amplitude w beyond the statement that it vanishes to leading order.

Section [III D 1](#) introduces defect measures at the level of generalities for effectively planar shells. Then in Section [III D 2](#) we derive a variational principle and boundary value problem they satisfy. Various properties of elastic patterns can be deduced. For instance, we explain in Section [III D 3](#) how to rule out the meeting of ordered wrinkles where the Gaussian curvature $\kappa \geq 0$. The reader looking for a concrete example should see Section [III E](#) where we solve for the defect measure and displacements of a positively curved ellipse.

1. Defect measures and asymptotic isometries

Our starting point is the question of how to pass to the limit in the statement that asymptotic isometries have vanishingly small strain, i.e.,

$$\varepsilon = e(u) + \frac{1}{2} \nabla w \otimes \nabla w - \frac{1}{2} M \rightarrow 0. \quad (\text{S30})$$

Of course, the effective strain $\varepsilon_{\text{eff}} = e(u_{\text{eff}}) - \frac{1}{2} M$ need not vanish due to the presence of geometric incompatibilities. Since $\varepsilon_{\text{eff}} \leq 0$, the deviation $\varepsilon - \varepsilon_{\text{eff}}$ tends towards a non-negative quantity. Where it is other than zero some pattern forms. The notion of defect measure $\mu(dx)$ serves to make its limiting features precise.

Referring back to Section [III A](#) and in particular [\(S12\)](#) and [\(S13\)](#), we see that states $(u, w) \rightarrow (u_{\text{eff}}, 0)$ with energy scaling as the minimum must satisfy $\int_{\Omega} |\nabla w|^2 \lesssim 1$, meaning that their out-of-plane displacement gradients are bounded *a priori* in mean-square. This permits defining the “defect measure” $\mu(dx)$ of the accompanying pattern through the limiting procedure

$$\nabla w \otimes \nabla w \rightharpoonup \langle \nabla w \otimes \nabla w \rangle := \mu(dx) \quad (\text{S31})$$

where the half-arrow indicates the following “asymptotic averaging” operation: exchange the limit $\gamma_{\text{eff}} \rightarrow 0$ for an integral against a non-negative two-by-two symmetric tensor $\mu(dx)$ satisfying

$$\int_{\Omega} \zeta : \nabla w \otimes \nabla w \, dx \rightarrow \int_{\Omega} \zeta : \mu(dx)$$

regardless of the choice of “test” field $\zeta(x)$. The exchange can be thought of in analogy with the use of ergodicity to relate space and time averages, with the limit playing the role of a long-time evolution and the choice of test field representing a particular statistic that is preserved. Here it suffices to test against continuous ζ vanishing at the boundary of the shell (this defines the so-called weak-* convergence used in [\[1\]](#)). Defect measures are only one of many such devices that have been developed to describe patterns governed by nonlinear partial differential equations (see, e.g., [\[19\]](#)). The terminology is nicely illustrative of an analogy between elastic patterns and material defects such as voids, each of which provides a route to accommodating effective strain.

With the defect measure μ in hand, we can now easily obtain from [\(S30\)](#) the *limiting isometry* equation

$$\varepsilon_{\text{eff}} + \frac{1}{2} \mu = 0 \quad \text{where} \quad \mu(dx) = \langle \nabla w \otimes \nabla w \rangle. \quad (\text{S32})$$

This important equation makes precise the coupling between elastic patterns and effective strains. The notation dx reminds that defect measures are defined both for “continuous” and “singular” patterns, reflecting the distinct possibilities of wrinkles where material accumulates in a diffuse manner across the shell, or folds where material collects along distinguished curves (the latter is marked by a singular, Dirac-like concentration in μ). One of the results of the ensuing analysis is to rule out the existence of folds in the ordered region of shallow shells. This is consistent with our use of the von Karman-like expression for the strain in [\(S30\)](#), which can be expected to fail when the misfit M becomes too large. For examples of folds in non-shallow shells see [\[20\]](#).

2. A boundary value problem for defect measures

Here we derive a boundary value problem characterizing the defect measures $\mu(dx)$ of effectively planar shells. First, we identify a variational principle they satisfy. The key is to relate the “mass” of the defect measure to the areal change ΔA from the maximum coverage problem [\(S16\)](#). Taking the trace of the limiting isometry equation [\(S32\)](#) and using [\(S10\)](#) yields

$$\Delta A = \frac{1}{2} \int_{\Omega} |\mu|_1$$

where $|\cdot|_1$ indicates a sum of singular values. Minimizing over tension-free effective displacements $u_{\text{eff}}(x)$ is the same as minimizing over defect measures $\mu(dx)$. For simply connected shells,

$$\min_{\substack{u_{\text{eff}}(x) \\ \varepsilon_{\text{eff}} \leq 0}} \Delta A = \min_{\substack{\mu(dx) \geq 0 \\ -\frac{1}{2} \text{curlcurl } \mu = \kappa}} \frac{1}{2} \int_{\Omega} |\mu|_1 \quad (\text{S33})$$

where the constraints on μ ensure the solvability of [\(S32\)](#) for tension-free u_{eff} according to the Saint-Venant compatibility conditions for linear strains. Additional integral constraints arise for multiply connected shells. This variational principle has the appealing interpretation of minimizing over compatible patterns. Leveraging the coarse-graining results from Section [III A 3](#) (see page [S8](#) for a summary) we conclude that any optimal μ solving [\(S33\)](#) arises from a sequence of ground or near ground states of the original energy U ; moreover, all such sequences necessarily produce optimal μ .

We come now to the boundary value problem for defect measures. Combining the Saint-Venant compatibility conditions with the complementary slackness conditions [\(S28\)](#) expressed via [\(S32\)](#), we deduce the following powerful result (stated first for simply connected shells):

a non-negative two-by-two symmetric tensor $\mu(dx) \geq 0$ arises as the defect measure of ground or near ground states if and only if

$$\begin{cases} -\frac{1}{2} \operatorname{curl} \operatorname{curl} \mu = \kappa & \text{in } \Omega \\ \sigma_L : \mu = 0 & \text{in } \Omega \\ \hat{\nu} \cdot (x - \nabla \varphi) \mu_{\hat{\tau} \hat{\tau}} = 0 & \text{at } \partial \Omega \end{cases} \quad (\text{S34})$$

We view (S34) as a boundary value problem for μ with data set by the curvature $\kappa(x)$, the planform Ω , and the locking stress σ_L which of course depends on the first two. The first equation expresses elastic compatibility — with asymptotic isometries — and reflects Gauss' *Theorema Egregium* at the level of the patterns. The second and third equations comprise the full set of complementary slackness conditions equivalent to the optimality of φ and μ (likewise σ_L and ε_{eff}). As usual, $\hat{\nu}$ and $\hat{\tau}$ denote the outwards pointing normal and tangent vectors at $\partial \Omega$.

We have stated (S34) for simply connected shells to keep the exposition tight. There is a multiply connected version as well. The first equation must be altered to account for holes, as is usual with compatibility conditions. The second equation remains the same. The third equation must be restated and becomes

$$(\sigma_L)_{\hat{\tau} \hat{\tau}} \mu_{\hat{\tau} \hat{\tau}} = 0 \quad \text{at } \partial \Omega \quad (\text{S35})$$

for general shells. The coefficient records the tangential boundary component of the concentrated part of σ_L . It can be evaluated as $(\sigma_L)_{\hat{\tau} \hat{\tau}} = \hat{\nu} \cdot [\nabla \varphi]$ where $[\cdot]$ reports the value of a jump. For multiply connected shells, the Airy potential φ differs from $\frac{1}{2}|x|^2$ outside Ω up to a locally affine function. In the simply connected case, we may simply take $\varphi = \frac{1}{2}|x|^2$ outside Ω as only its second derivatives enter in the locking stress. This leads to the formula $(\sigma_L)_{\hat{\tau} \hat{\tau}} = \hat{\nu} \cdot (x - \nabla \varphi)$ and recovers (S34). The reader may note that this choice is what underlies the relaxed boundary conditions (S26).

Various striking conclusions can be drawn regarding elastic patterns using the boundary value problem just derived. If, for instance, it turns out that for some curvature κ and planform Ω only a single solution μ exists, one would learn that all ground and near ground states agree to leading order. If instead multiple solutions exist, there would exist multiple distinct near ground states. In the presence of stable lines we have established certain partial uniqueness results showing, essentially, that all solutions μ agree upon restriction to the ordered part $\sigma_L \neq 0$. We have also shown that they are regular there, ruling out the existence of folds in the ordered part. In the other direction, we have constructed infinitely many solutions for a positively curved disc, using the fact that it lacks any stable lines and is (generically) totally disordered. Thus, a positively curved disc admits infinitely many distinct near ground states. The question remains whether there are as many ground states. See [1, Sects. 5,6] for various precise statements of these results.

3. On the sign of curvature where ordered wrinkles meet

A key realization permitting the solution of the boundary value problem for defect measures $\mu(dx)$ is that it can be treated using the method of characteristics with stable lines as characteristic curves. The method of characteristics is a classic method for solving partial differential equations by reducing them to ordinary differential equations along curves (see, e.g., [21]). Our fundamental realization is that the stable lines of an effectively planar shell — its asymptotic wrinkle peaks and troughs — are nothing other than characteristic curves for Gauss' *Theorema Egregium* at the level of μ .

To demonstrate the power of this idea, we show now how to rule out the meeting of distinct families of ordered wrinkles transverse to any interior curve $\Sigma \subset \Omega$ where the curvature $\kappa(x) \geq 0$. This is consistent with the appearance of distinguished curves where wrinkles meet in negatively curved shells (the medial axes in Figures 1 and 2 of the main text). It also helps explain the appearance of “leftover” parts not filled by orderly wrinkles in generic positively curved shells. The result is, of course, far more general than these examples as it holds without any assumptions on κ away from the curve.

To prove it, we simply need to ask what is implied by the system (S34) where distinct families of ordered wrinkles meet. We understand the statement that they belong to “distinct families” to mean that their stable lines descend from a singular Airy potential φ . In terms of the locking stress σ_L , we mean for it to concentrate along the curve Σ across which the gradient of its Airy potential exhibits a jump $[\nabla \varphi] \neq 0$. We note it would be too restrictive to simply assume that the direction of wrinkling changes sharply at Σ (here, we have in mind the middle part of the negatively curved rectangle from Figure 2 of the main text).

Recall stable lines are defined in the ordered part $\sigma_L \neq 0$ as lines passing through a principal direction of positive locking stress $\hat{T}(x)$. The asymptotic wrinkle direction is perpendicular to the stable lines as was shown in Section III B. Hence,

$$\mu_{\hat{T} \hat{T}} = \hat{T} \otimes \hat{T} : \langle \nabla w \otimes \nabla w \rangle = \langle |\hat{T} \cdot \nabla w|^2 \rangle = 0$$

yielding for the full defect measure

$$\mu = \langle |\hat{T}^\perp \cdot \nabla w|^2 \rangle \hat{T}^\perp \otimes \hat{T}^\perp$$

where again $\langle \cdot \rangle$ denotes the *asymptotic* averaging defined in (S31). Orient the stable lines to point away from Σ thereby fixing the direction of \hat{T} . Applying the method of characteristics to the first part of (S34) then yields the ordinary differential equation

$$-\frac{1}{2\varrho} \partial_{\hat{T}}^2 (\varrho \mu_{\hat{T}^\perp \hat{T}^\perp}) = \kappa \quad \text{along stable lines.} \quad (\text{S36})$$

The shorthand $\partial_{\hat{T}} = \hat{T} \cdot \nabla$ denotes a directional derivative along stable lines. The term $\varrho(x) > 0$ is a change-of-variables factor arising in a passage from the original

Euclidean coordinates to ones adapted to the lines. It can be determined by solving the equation

$$\partial_{\hat{T}} \varrho = \operatorname{div} \hat{T} \varrho$$

involving their “splay” $\operatorname{div} \hat{T}$.

Now we invoke the assumptions of distinct families and transversality. As a result, the locking stress σ_L concentrates $\sim \hat{\nu}_\Sigma \cdot [\nabla \varphi] \hat{\tau}_\Sigma \otimes \hat{\tau}_\Sigma \neq 0$ along Σ , where $\hat{\nu}_\Sigma$ denotes a unit normal to this curve. The tangent direction $\hat{\tau}_\Sigma$ remains non-parallel to \hat{T} , since otherwise the wrinkles do not meet Σ transversely. Manipulation of the first and second equations in (S34) yield the matching conditions

$$\begin{aligned} |\hat{\nu}_\Sigma \cdot [\nabla \varphi]| |\hat{\tau}_\Sigma \cdot \hat{T}^\perp|^2 \cdot \varrho \mu_{\hat{T}^\perp \hat{T}^\perp} = 0 & \quad \text{at } \Sigma \\ \text{and } \partial_{\hat{T}} (\varrho \mu_{\hat{T}^\perp \hat{T}^\perp}) = 0 & \quad \text{at } \Sigma, \end{aligned} \quad (\text{S37})$$

the coefficients of which were just shown to be non-zero. Combining this with (S36) yields the Taylor expansion

$$\mu_{\hat{T}^\perp \hat{T}^\perp} = -\kappa(x_0) \left((x - x_0) \cdot \hat{T} \right)^2 + \dots \quad \text{for } x \approx x_0 \in \Sigma.$$

Evidently, $\mu_{\hat{T}^\perp \hat{T}^\perp}$ and κ are of opposite signs. Where there is a pattern, $\mu_{\hat{T}^\perp \hat{T}^\perp} = \langle |\partial_{\hat{T}^\perp} w|^2 \rangle > 0$. Hence, $\kappa < 0$ along curves where ordered wrinkles meet. If $\kappa \geq 0$ no such meeting can occur. See [1, Sect. 5] for more details, including an analysis leading to the same conclusion that $\kappa < 0$ where ordered wrinkles meet at a point.

E. Worked example: a positively curved ellipse

When a positively curved ellipse is pressed into the plane, it responds with a pattern of wrinkles propagating along a constant direction with amplitude as shown in Figure 3 of the main text. This section shows how to deduce the response by applying the methodology developed above. Numerous other worked examples can be found in [1, Sect. 6]. We assume the reader is familiar with the concepts introduced in Section III A–Section III D, namely the effective strain $\varepsilon_{\text{eff}}(x) = e(u_{\text{eff}}) - \frac{1}{2}M$ with misfit M , the locking stress $\sigma_L(x)$, its convex Airy potential $\varphi(x)$, and finally the defect measure $\mu(dx)$.

Consider a shallow shell with an elliptical planform

$$E = \left\{ (x_1, x_2) : \frac{x_1^2}{\epsilon^2 W^2} + \frac{x_2^2}{W^2} < 1 \right\}$$

having positive Gaussian curvature

$$\kappa(x) = \det \nabla \nabla p(x) > 0.$$

Take $\epsilon > 1$ so that the x_1 -coordinate runs along the major axis of the ellipse. We are interested in determining the pattern (or, in principle at first, patterns) that arise when the shell is pressed flat. The first step is to determine the stable lines throughout the ordered part. Once these are known, the pattern is set and the displacements of the shell can be found.

Solving the locking stress problem — either in its original ill-posed form (S25), or in its relaxed Airy potential form for simply connected shells in (S27) — we find that the locking stress of a positively curved ellipse satisfies

$$\sigma_L(x) = \left(1 - \frac{1}{\epsilon^2} \right) \hat{e}_2 \otimes \hat{e}_2 \quad (\text{S38})$$

throughout the planform E . It also concentrates at ∂E , a fact we will return to clarify later on below. The ellipse presents a completely ordered response with stable lines parallel to its minor axis. These claims follow from the results of Section III C 2 as we briefly explain. Since $\kappa(x) > 0$, the optimal Airy potential is the largest convex extension $\varphi_+ \circ \frac{1}{2}|x|^2$ into E , with the explicit formula

$$\varphi_+(x) = \frac{1}{2} \left(W^2 + \left(1 - \frac{1}{\epsilon^2} \right) x_1^2 \right). \quad (\text{S39})$$

The following geometric construction permits a simple proof: identify the ellipse E as a tangential region with inscribed circle C centered at its origin $x = 0$. The contact region built from where C contacts E degenerates to its minor axis, and the remainder is covered by lines parallel to it. This is enough to verify (S38) and (S39). Of course, the formal argument involves checking the optimality of the proposed stable lines via (S29), but this is not so difficult to do with the picture in mind.

Next we determine the amplitude of the response. To leading order, the out-of-plane displacement $w(x) \approx 0$ as explained in Section III A 3 c. Here, we compute its defect measure $\mu(dx) = \langle \nabla w \otimes \nabla w \rangle$ which is coupled to the effective strain via $\varepsilon_{\text{eff}} + \frac{1}{2}\mu = 0$, see (S32). Again, the brackets $\langle \cdot \rangle$ denote an asymptotic averaging over small scales. We think of μ as providing the mean-square amplitude of w asymptotically up to a rescaling as $w \rightarrow 0$. Using that the locking stress and effective strain are orthogonal as per (S23), it follows here that

$$(\varepsilon_{\text{eff}})_{22} = \hat{e}_2 \otimes \hat{e}_2 : \varepsilon_{\text{eff}} = \left(1 - \frac{1}{\epsilon^2} \right)^{-1} \sigma_L : \varepsilon_{\text{eff}} = 0.$$

Therefore, $\mu_{22} = \langle |\partial_2 w|^2 \rangle = 0$ reflecting an arrangement of stable lines parallel to the principal direction of locking stress \hat{e}_2 . The full defect measure takes the form

$$\mu = \langle |\partial_1 w|^2 \rangle \hat{e}_1 \otimes \hat{e}_1 \quad (\text{S40})$$

with its only non-zero component $\mu_{11} = \langle |\partial_1 w|^2 \rangle$ being governed by the first and third equations in the boundary value problem (S34). (The second equation was used when we invoked the orthogonality of stress and strain.) These can be solved using the method of characteristics as anticipated in Section III D 3. Before getting to specifics, let us outline the general approach.

First, we recall from (S36) that the partial differential equation in (S34) can be rewritten as the ordinary differential equation

$$-\frac{1}{2\varrho} \partial_{\hat{T}}^2 (\varrho \mu_{\hat{T}^\perp \hat{T}^\perp}) = \kappa \quad \text{along stable lines.} \quad (\text{S41})$$

The vector field $\hat{T}(x)$ is a principal direction of locking stress, i.e., a direction parallel to the stable lines. The parallel and perpendicular components of μ satisfy

$$\mu_{\hat{T}\hat{T}} = \langle |\partial_{\hat{T}} w|^2 \rangle = 0 \quad \text{and} \quad \mu_{\hat{T}^\perp \hat{T}^\perp} = \langle |\partial_{\hat{T}^\perp} w|^2 \rangle > 0$$

with the strict inequality indicating a pattern. Integrating (S41) yields a formula for $\mu_{\hat{T}^\perp \hat{T}^\perp}$ once appropriate boundary conditions are supplied. In the present positively curved example stable lines extend between boundary points. Generally speaking, in such a situation we can apply the third part of (S34), or (S35) in the multiply connected case, to deduce that

$$|\hat{\nu} \cdot [\nabla \varphi]| |\hat{\tau} \cdot \hat{T}^\perp|^2 \cdot \varrho \mu_{\hat{T}^\perp \hat{T}^\perp} = 0 \quad \text{at } \partial\Omega \quad (\text{S42})$$

where $\hat{\nu}$ and $\hat{\tau}$ are the outwards pointing unit normal and tangent vectors. This is completely analogous to the matching conditions (S37), which apply in cases of negative curvature where stable lines meet in the bulk. The term $\varrho(x) > 0$ is a change-of-variables factor satisfying $\partial_{\hat{T}} \varrho = \text{div} \hat{T} \varrho$. So long as the coefficients in (S42) are non-zero, $\varrho \mu_{\hat{T}^\perp \hat{T}^\perp} = 0$ at $\partial\Omega$. Combining this with (S41) produces a more or less explicit formula for μ .

Back to the positively curved ellipse. Recall its locking stress was shown in (S38) to have the principal positive direction $\hat{T} = \hat{e}_2$ dictating parallel stable lines. So, ϱ is a constant and, as the lines fill the planform, $\varrho = 1$. Note $\hat{\nu} \cdot [\nabla \varphi] = \hat{\nu} \cdot (x - \nabla \varphi_+) > 0$ at the boundary due to (S39), reflecting a concentration in the locking stress $\sim \hat{\nu} \cdot [\nabla \varphi] \hat{\tau} \otimes \hat{\tau} \neq 0$ there. The stable lines meet it transversely so $|\hat{\tau} \cdot \hat{T}^\perp| = |\hat{\tau} \cdot \hat{e}_1| > 0$. Thus, the first and third equations from the original boundary value problem (S34) boil, via (S41) and (S42), down to the system

$$\begin{cases} -\frac{1}{2} \partial_2^2 \mu_{11} = \kappa & \text{in } E \\ \mu_{11} = 0 & \text{at } \partial E \end{cases} \quad (\text{S43})$$

for the mean-square amplitude $\mu_{11} = \langle |\partial_1 w|^2 \rangle$. This can be easily integrated and combined with (S40) to determine μ uniquely and explicitly throughout. After that, an approximation for w can be produced. The effective in-plane displacement u_{eff} can be recovered from integrating the equation $e(u_{\text{eff}}) - \frac{1}{2}M = \varepsilon_{\text{eff}} = -\frac{1}{2}\mu$.

We finish by showing how to approximate w in the case that the Gaussian curvature is constant, with $\kappa = R^{-2}$. Integrating (S43) shows that the unique defect measure for a constant positively curved ellipse is

$$\mu(dx) = \left(\frac{W}{R} \right)^2 \left(1 - \frac{x_1^2}{\epsilon^2 W^2} - \frac{x_2^2}{W^2} \right) \hat{e}_1 \otimes \hat{e}_1. \quad (\text{S44})$$

The statement that μ is unique implies that all ground and near ground states are to leading order identical. As μ lacks any Dirac-like part, folds concentrating along curves are ruled out in favor of a diffuse pattern. (In fact, these properties hold for general positively curved

ellipses, since (S43) has a unique solution lacking concentration in any case.) The simplest example of an out-of-plane displacement consistent with (S44) has

$$w(x) \approx \frac{W}{R} \sqrt{1 - \frac{x_1^2}{\epsilon^2 W^2} - \frac{x_2^2}{W^2}} \cdot \frac{\lambda}{\sqrt{2\pi}} \cos \left(\frac{2\pi}{\lambda} x_1 + \phi \right)$$

indicating wrinkles at a wavelength λ and phase ϕ not specified at this level of description. Fitting these to simulation data yields the theoretical curve (black) in Figure 3 of the main text. Outside of a small rim, the prediction is in excellent agreement with the actual response.

F. Future directions

The methods developed here constitute a general toolkit for deducing the coarse-grained aspects of wrinkle patterns arising in situations of geometrically incompatible confinement. Nevertheless, questions remain and in particular we highlight a need for understanding the sensitivity of wrinkle patterns to perturbations of shape, as well as the appearance of what we refer to as “incidental” order in regions predicted to be disordered otherwise. For other, more mathematically oriented questions we refer to the introduction of [1].

1. Sensitivity to perturbations of shape

Figure S3a shows a series of experiments with circular and elliptical shells cut out of a spherical cap of fixed radius of curvature. The major axis is kept fixed and the minor axis is made shorter from left to right. The circle on the far left presents a disordered response, while the ellipse on the far right is ordered. The ellipse in the middle shows a disordered response. Thus, although the asymptotic calculations from Section III E predict an ordered response for any non-zero ellipticity, experimentally we find that there is a finite threshold which must be exceeded for ordered wrinkles to appear. This threshold is observed to be comparable to other small yet finite lengths, such as the wrinkle wavelength and the width of the tensional rim. Future work should elucidate the physical balance underlying this transition.

Likewise, Figure S3b shows a series of experiments where a strip is removed from a spherical shell. The leftmost image shows a disc with no strip removed. It exhibits a disordered response. After a threshold amount is cut a transition occurs to an ordered response, wherein wrinkles follow a radial pattern of lines. This pattern is predicted by the circumscribed circle construction (see Section III C 2) albeit for any positive cut. The experiments suggest the shell becomes ordered when the width of the removed strip is equal to that of the tensional rim.

2. Order in generically disordered regions

We sometimes observe ordered, repeatable patterns in regions predicted to be consistent with disorder. Examples appear in Figure 4c of the main text as well as in Figure S4a. Such ordering is, however, observed to be “incidental” in that it is not the generic response. We note it does not contradict our theoretical predictions concerning the possibility of disorder where the locking stress $\sigma_L = 0$, as when this occurs the energy of the shell is shown to be insensitive to the local direction of wrinkling at leading order. This indicates, though does not immediately prove, the possibility of a multitude of ground or near ground states corresponding to distinct defect measures. We highlight the case of a positively curved disc, which is known to exhibit infinitely many near ground states [1, Sect. 6].

One wonders under what circumstances incidental order presents. Empirically, we find that it occurs when the wrinkle wavelength is not well-separated from the width of the potentially disordered region. Figure S4b shows a central region with more disorder than the analogous region in Figure S4a, which is presumably brought on by the larger ratio of its width to that of the wrinkles. An exploration of this should be the subject of future work.

IV. MATERIALS AND METHODS

A. Film preparation

We spin-coat solutions of polystyrene in toluene onto glass substrates of various positive and negative Gaussian curvatures. Film thickness is varied by changing the polymer concentration (1 to 5% by mass) and spinning speed (2000 to 4000 rpm). Different shapes are cut out using a metal scribe. After preparing the glass substrates with a thin layer of poly(acrylic acid), the films are released by dissolving this sacrificial layer in water. The films are finally transferred to a pure water-air interface. Following the experiments, each film is captured and its thickness is measured using a white-light interferometer (Filmetrics F3).

B. Finite element simulations

Simulations of shells bonded to a planar liquid substrate without surface tension are performed using the finite element package ABAQUS/Explicit. Four-node thin shell elements with reduced integration (element type S4R) are used. The confining force is specified as a non-uniform distributed pressure load over the surface of the shell, via a VDLOAD subroutine. Free boundary conditions are used. Comparative non-linear geometric finite element analysis using both linearly elastic and

neo-Hookean hyperelastic materials show the results are largely independent of the model. Color-coding in the images correspond to vertical deflections from the plane.

C. Parameter ranges

Here we report the parameter ranges of the 111 experiments and several hundred simulations in our study. For specific parameters corresponding to the images in the main text and in Section II, see the tables in Section I and the figure captions, respectively. We use the dimensionless groups (S2) to report the ranges, which we recall for the reader’s convenience are the inverse bendability $b = BR^2/YW^4$, inverse deformability $k = KR^2/Y$, and inverse confinement $\gamma = \gamma_{lv}R^2/YW^2$.

Let us comment briefly on the relation between the parameter regime used in our derivation of the maximum coverage problem in Section III A and the tested ranges. While the condition (S3) is satisfied in the experiments and simulations, the extra hypothesis (S7) fails. Nevertheless, the results make clear that the maximum coverage problem captures the wrinkle patterns of confined elastic shells far beyond the validity of this hypothesis. It seems that some even more general route to deriving the maximum coverage problem is yet to be found.

1. Experimental ranges

The shells are shallow with $0.01 < (W/R)^2 < 0.2$ and highly bendable with $4 \times 10^{-11} < b < 2 \times 10^{-8}$. The substrate has non-dimensional stiffness $0.003 < k < 0.03$. Regarding the regime (S3), the experiments satisfy

$$10^{-2} < \frac{\gamma}{k} < 0.7, \quad 10^{-6} < 2\sqrt{bk} < 3 \times 10^{-5}, \\ 4 \times 10^{-4} < \gamma < 10^{-2}, \quad 10^{-3} < (b/k)^{1/4} < 10^{-1}.$$

Since $2\sqrt{bk} + \gamma \approx \gamma$ the effective tension $\gamma_{\text{eff}} \approx \gamma_{lv}$.

2. Simulation ranges

The shells are shallow with $0.01 < (W/R)^2 < 0.04$ and highly bendable with $7 \times 10^{-9} < b < 2 \times 10^{-6}$. The substrate has non-dimensional stiffness $6 < k < 40$ and the surface tension is zero by design. Regarding the regime (S3), the simulations satisfy

$$\frac{\gamma}{k} = 0, \quad 2 \times 10^{-4} < 2\sqrt{bk} < 2 \times 10^{-2}, \\ \gamma = 0, \quad 5.6 \times 10^{-3} < (b/k)^{1/4} < 10^{-2}.$$

The effective tension $\gamma_{\text{eff}} = 2\sqrt{BK}$.

[1] I. Tobasco, [arXiv:1906.02153](https://arxiv.org/abs/1906.02153).

[2] J. L. Sanders, Jr., *Quart. Appl. Math.* **21**, 21 (1963).

[3] E. Ventsel and T. Krauthammer, *Thin plates and shells: Theory, analysis, and applications* (CRC press, 2001).

[4] P. Howell, G. Kozyreff, and J. Ockendon, *Applied solid mechanics* (Cambridge University Press, Cambridge, 2009).

[5] E. Efrati, E. Sharon, and R. Kupferman, *J. Mech. Phys. Solids* **57**, 762 (2009).

[6] E. Hohlfeld and B. Davidovitch, *Phys. Rev. E* **91**, 012407 (2015).

[7] M. Taffetani and D. Vella, *Philos. Trans. Roy. Soc. A* **375**, 20160330 (2017).

[8] J. Chopin, V. Démery, and B. Davidovitch, *J. Elasticity* **119**, 137 (2015).

[9] D. Vella, J. Huang, N. Menon, T. P. Russell, and B. Davidovitch, *Phys. Rev. Lett.* **114**, 014301 (2015).

[10] B. Davidovitch, Y. Sun, and G. M. Grason, *Proc. Natl. Acad. Sci.* **116**, 1483 (2019).

[11] B. Audoly and A. Boudaoud, *J. Mech. Phys. Solids* **56**, 2422 (2008).

[12] R. V. Kohn and H.-M. Nguyen, *J. Nonlinear Sci.* **23**, 343 (2013).

[13] A. Braides, *Γ -convergence for beginners* (Oxford University Press, Oxford, 2002).

[14] G. Dal Maso, *An introduction to Γ -convergence* (Birkhäuser Boston, Inc., Boston, MA, 1993).

[15] W. Prager, *Trans. Soc. Rheol.* **1**, 169 (1957).

[16] D. J. Struik, *Lectures on classical differential geometry* (Dover Publications, Inc., New York, 1988).

[17] M. P. do Carmo, *Differential geometry of curves & surfaces* (Dover Publications, Inc., Mineola, NY, 2016).

[18] H. King, R. D. Schroll, B. Davidovitch, and N. Menon, *Proc. Natl. Acad. Sci.* **109**, 9716 (2012).

[19] P. Gérard, *Comm. Partial Differential Equations* **16**, 1761 (1991).

[20] O. Albarrán, D. V. Todorova, E. Katifori, and L. Goehring, [arXiv:1806.03718](https://arxiv.org/abs/1806.03718).

[21] L. C. Evans, *Partial differential equations* (American Mathematical Society, Providence, RI, 2010).